Chapter 11
Integrating X-ray CT Data into Models

Xavier Portell, Valerie Pot, Ali Ebrahimi, Olivier Monga, and Tiina Roose

11.1 Introduction

X-ray Computed Tomography (X-ray CT) offers important 4-D (i.e., 3-D scanning over time) structural information of the soil architecture. This imaging tool provides access to the 3-D morphological properties of the soil pore space such as the 3-D connectivity of pores that are essential to the understanding of water, solute, and gas transport processes. Other morphological properties such as pore-size distribution,

X. Portell (✉)
School of Water, Energy and Environment, Cranfield University, Bedfordshire, UK

Departamento de Ciencias, IS-FOOD, Universidad Pública de Navarra, Pamplona, Spain
e-mail: xavier.portell@unavarra.es

V. Pot
Université Paris-Saclay, INRAE, AgroParisTech, UMR ECOSYS, Palaiseau, France
e-mail: Valerie.Pot@inrae.fr

A. Ebrahimi
Department of Civil and Environmental Engineering, Massachusetts Institute of Technology, Cambridge, MA, USA
e-mail: alieb@mit.edu

O. Monga
Sorbonne Université, IRD, UMMISCO, Bondy, France
e-mail: olivier.monga@ird.fr

T. Roose
Bioengineering Sciences Research Group, Department of Mechanical Engineering, School of Engineering, Faculty of Engineering and Physical Sciences, University of Southampton, Southampton, UK
e-mail: t.roose@soton.ac.uk

specific surface area, or spatial heterogeneity of soil can be obtained from the X-ray CT images. Many studies have used this technique to better understand the evolution of macroscopic soil physical properties such as structural stability and relate it to spatial descriptors of soil pore space morphology when the soil undergoes wetting/drying cycles (e.g., Diel et al., 2019) or when it is subjected to different agricultural practices (e.g., Papadopoulos et al., 2009; Dal Ferro et al., 2013; Caplan et al., 2017). Non-equilibrium transfer processes, such as preferential transport, have also been related to the quantification of macropores in X-ray CT images (e.g., Larsbo et al., 2014; Katuwal et al., 2015; Soto-Gómez et al., 2018). In addition, X-ray CT data have proved particularly useful for reconstructing the skeletons of biopore networks, such as those burrowed by earthworms (Capowiez et al., 1998), and for monitoring their temporal dynamics (Joschko et al., 1993) (see Chap. 10). The role of air-filled soil pores and in particular their connectivity in 3-D in the transport of microbial-generated gaseous products (N_2O, CO_2) have been hypothesized (Rabot et al., 2015; Porre et al., 2016). X-ray CT data have also provided new knowledge about the 3-D architecture of root systems (e.g., Helliwell et al., 2013) and their impact on the 3-D soil architecture (see Chap. 9). For instance, root hairs were shown to modify the pore-size distribution and connectivity in the rhizosphere (e.g., Keyes et al., 2013; Koebernick et al., 2017, 2019). X-ray CT measurements have also allowed imaging aerenchymatous roots and the gas bubbles entrapped in the soil of rice paddies to explain transport of CO_2 and O_2 between roots and the atmosphere (Kirk et al., 2019). The dynamics of the spatial dispersion of soil microorganisms could be related to the 3-D description of the pore space obtained by X-ray CT (Juyal et al., 2020). The role of some pore-size classes could also be linked with soil carbon storage (Kravchenko et al., 2020) (see Chap. 10).

Many experimental studies have highlighted the link between soil functioning and structural information of soil architecture extracted from X-ray CT. This is often performed by looking for correlations between measured soil functions and morphological properties of the pore space. From this vantage point, modelling offers an interesting and complementary methodological tool to these studies. In addition to their predictive character, models open the way to the testing of hypotheses about the role of the complex soil architecture on soil biological and physical processes, by carrying out structurally realistic *in-silico* experiments that can now be set up thanks to X-ray CT imaging. Development of spatially explicit pore-scale modelling in the 1990s, encompassed with a steep increase in desktop processors computing power and development of parallel computing algorithms, has made the routine use of X-ray CT images in modelling common. Early examples of the integration of X-ray CT data into spatially explicit models are found in the rock physics domain (Spanne et al., 1994; Hazlett, 1995). The inclusion of X-ray CT data into models focusing on soils occurred at a later stage (Falconer et al., 2005; Monga et al., 2008; Keyes et al., 2013). Consequently, the rock physics domain accounts for a large number of studies dealing with water flow, multiphase flow, and reactive transport (e.g., Blunt et al., 2013; Bultreys et al., 2016; de Paulo et al., 2020), whilst the soil domain has been the object of a lower number of studies, possibly because of its importance not being widely recognized and/or funding being more abundant for the problems

dealing with oil and gas movement in the rocks. Synthetic porous media or packing of sands have also been imaged and processed into pore-scale models to study fundamental physical and biological processes in granular media (e.g., Schaap et al., 2007; Sukop et al., 2008; Peszynska et al., 2016). Such approaches are a valuable step forward to account for some of the soil complexity, but outputs obtained should be taken cautiously because the studied system can behave fundamentally differently from the real soil situation.

The main approach in using X-ray CT information in image-based models is the direct integration of the 3-D organization of the soil phases in the numerical grid of pore-scale models. Soil processes such as water flow, multiphase flow, diffusion, or reactive transport are subsequently computed in the 3-D pore space using Computational Fluid Dynamics (CFD) tools such as Finite-Element, Finite-Volume, or lattice-Boltzmann approach. In an alternative indirect approach, X-ray CT data is used to obtain key image-based structural qualities to parameterize soil features that are needed as input parameters into macroscopic soil models that ignore the explicit 3-D description of soil. One example of such a morphometric statistical approach is the extraction of critical pore diameters to be used in macroscopic analytical relations to predict saturated hydraulic conductivity. The structural morphometric parameters obtained from X-ray CT can also be used to generate an equivalent 3-D pore space, for instance extracting the Euler number (a number used for quantifying the connectivity of the pore space) to parameterize a pore network model (PNM). The latter approach is also classified as indirect. Soil structure can also be generated from explicit soil images by using more sophisticated statistical methods such as the Markov-chain Monte-Carlo method as performed by Wu et al. (2004). Although the images used in this latter work were 2-D thin sections, the method can be applied to X-ray CT data (Lin et al., 2020).

This chapter focuses on soil modelling approaches that make use of X-ray CT. Other porous media, such as carbonate rocks, sandstone, etc., have been thoroughly addressed in other reviews (e.g., Golparvar et al., 2021) to which readers are referred to. First, we focus on the practical aspects of the integration of X-ray CT data of the main soil phases into spatially explicit models highlighting the main approaches that can be used for such integration. We then provide an overview of how X-ray CT data has been integrated in soil modelling research distinguishing between work on a direct or an indirect use of X-ray CT.

11.2   Direct Integration of X-ray CT Data-Derived Soil Phases into Image-Based Models

In this section, we focus on the integration of X-ray CT data of the main soil phases, namely pore space (sect. 11.2.1), air and water (sect. 11.2.2), organic matter (sect. 11.2.3), and roots (sect. 11.2.4), highlighting the main modelling strategies that can be adopted.

A number of preliminary steps must be carried out before the integration of the soil phases in image-based models can be undertaken. These processes allow for the acquisition of a greyscale representation of the soil structural information that is usually segmented to produce binary images, i.e., black and white. Following this, the different soil phases are then labelled by different colours identifying solid particles and non-solid particles (pores), which are normally used by image-based models despite providing less signal information than greyscale images. Readers interested in segmentation and post-treatment processes are referred to Chaps. 5 and 6 along with the reviews of Iassonov et al. (2009) and Schlüter et al. (2014).

11.2.1   Integration of X-ray CT Data of Pore Space Geometry

Different strategies can be adopted to integrate the structural information of pore space geometry provided by the segmented X-ray CT images into image-based models. We will distinguish four strategies differing in the degree of simplification of the soil structural information and the immediacy of their use: voxel-based, finite-element meshing, morphological, and irregular PNM approaches. The main characteristics of these strategies are summarized in Fig. 11.1.

The most straightforward strategy is to make use of all the structural information elements provided by the image to reconstruct the numerical grid. Depending on the CFD tools used, two approaches can be distinguished, the so-called 'voxel-based' and 'finite-element' modelling techniques. Voxel-based models directly map the voxels of the segmented X-ray CT image to the model's numerical grid, as is typically done when using lattice-Boltzmann models. Depending on the desired degree of accuracy of the soil processes, the lattice-Boltzmann grid can be further refined (e.g., Sukop et al., 2008). Finite-Element solvers require the reconstruction of the numerical grid using more or less sophisticated meshing software (e.g., iso2mesh, Tran et al., 2020).

Another strategy is to reduce the number of computational elements of the segmented X-ray CT image while keeping key structural information, as performed by the so-called 'morphological' and 'irregular Pore Networks' models. In these cases, the integration of X-ray CT data requires a number of operations specific for each modelling approach. The main steps required are reported in Fig. 11.2. Morphological models approximate the complex pore space morphology with a set of simplified geometrical primitives such as balls (e.g., Hilpert & Miller, 2001; Vogel et al., 2005; Lehmann et al., 2006; Monga et al., 2008), ellipsoids or generalized cylinders (Ngom et al., 2012; Kemgue et al., 2019), located along the median axes of the pore space. This set of maximal balls recover the skeleton of the pore space. These balls also function as the nodes of an adjacency graph, which considers the neighbourhood information of each geometric primitive (e.g., balls) where the soil processes are locally computed (Monga et al., 2007). They can also be used to construct generalized cylinders or ellipsoids (Ngom et al., 2012; Kemgue et al., 2019). Like morphological models, irregular PNMs construct networks of nodes
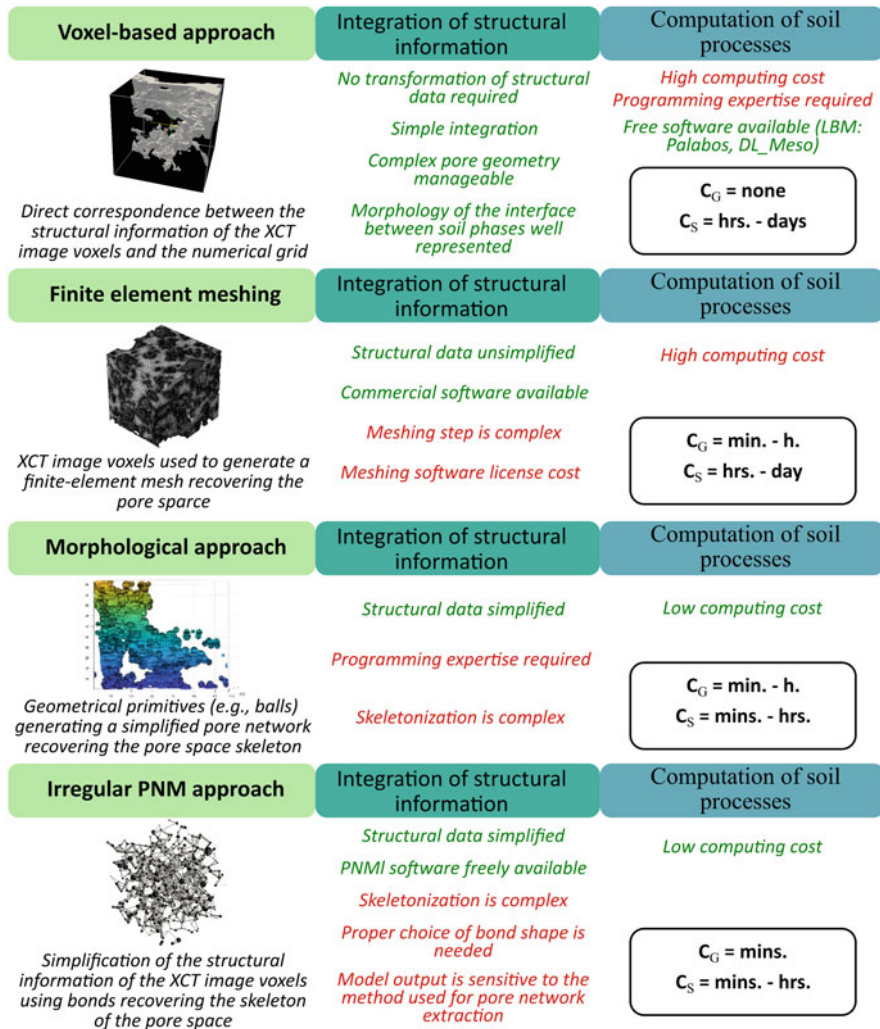
Voxel-based approach	Integration of structural information	Computation of soil processes
Direct correspondence between the structural information of the XCT image voxels and the numerical grid	*No transformation of structural data required* *Simple integration* *Complex pore geometry manageable* *Morphology of the interface between soil phases well represented*	*High computing cost* *Programming expertise required* *Free software available (LBM: Palabos, DL_Meso)* C_G = none C_S = hrs. - days
Finite element meshing	Integration of structural information	Computation of soil processes
XCT image voxels used to generate a finite-element mesh recovering the pore sparce	*Structural data unsimplified* *Commercial software available* *Meshing step is complex* *Meshing software license cost*	*High computing cost* C_G = min. - h. C_S = hrs. - day
Morphological approach	Integration of structural information	Computation of soil processes
Geometrical primitives (e.g., balls) generating a simplified pore network recovering the pore space skeleton	*Structural data simplified* *Programming expertise required* *Skeletonization is complex*	*Low computing cost* C_G = min. - h. C_S = mins. - hrs.
Irregular PNM approach	Integration of structural information	Computation of soil processes
Simplification of the structural information of the XCT image voxels using bonds recovering the skeleton of the pore space	*Structural data simplified* *PNMI software freely available* *Skeletonization is complex* *Proper choice of bond shape is needed* *Model output is sensitive to the method used for pore network extraction*	*Low computing cost* C_G = mins. C_S = mins. - hrs.

Fig. 11.1 Overview of four main methods used to integrate X-ray CT 3-D structural data in image-based models. In the figure, points that can be seen as advantages are in green while disadvantages are depicted in red. PNMs stands for pore network models. In the figure, C_G is an indication of the computing time required to *generate* the numerical grid and C_S is an indication of the computing time required to *simulate* diffusion of a chemical species through the network for 10 days. An X-ray CT image of 512^3 voxels and an average desktop computer (e.g., AMD Ryzen 7 or Intel i7 processor, and 16/32 GB of RAM) have been assumed on providing these indicative numbers

located along the median axes of the imaged pore space (e.g., Ebrahimi et al., 2013). Irregular PNMs use the same operations than the morphological approach to extract clusters of maximal balls. Then these clusters of maximal balls are converted to pore-throat network (Fig. 11.2). In both approaches, the size of the given geometrical
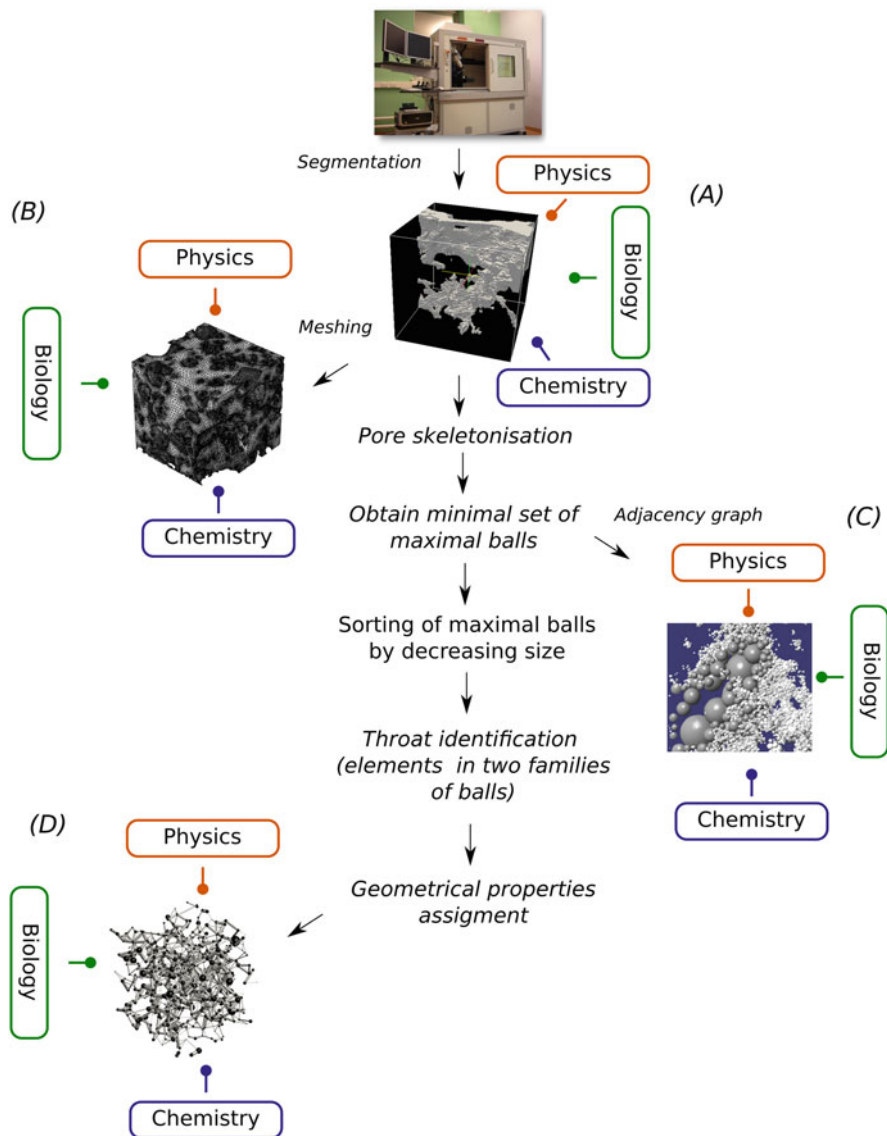
Fig. 11.2 Overview of the operations required to integrate X-ray CT images of the soil architecture into image-based models. For illustrative purpose, we sketch a binary segmented image showing pore and solid space. Note that other soil phases may be added (e.g., water phase, solid organic matter). (**a**) The segmented X-ray CT image is used directly by voxel-based approaches. Note that only the pore phase is represented in the figure. (**b**) Finite-element approaches use a mesh approaching where the segmented pore space is located. (**c**) The morphological approach requires the skeletonization of the segmented pore space image, which is used as a base to construct a minimal set of maximal balls that approach the soil pore space. Once identified, the relationships and connectivity of the maximal balls are written in an adjacency graph, which is valuated by attaching to each ball a set of attributes (e.g., air or water, organic matter mass). (**d**) In addition to the steps described by the morphological approach, irregular pore networking models extract clusters of maximal balls that are converted to pore-throat networks. This requires sorting the maximal balls by

primitives (in morphological models) and the bonds (in irregular PNMs) are locally computed from the measured area of inscribed circles or balls within the pores (e.g., Perez-Reche et al., 2012). PNMs classically use cylindrical or angular bonds (throats). There are standalone open software tools (http://openpnm.org, Gostick et al., 2016; http://porespy.org, Gostick et al., 2019) that allow constructions of these irregular pore networks.

In PNMs, the choice of the bond shape can have important consequences on the model behaviour. Microscopic soil images revealed that natural soil pores consist of heterogeneous and angular cross-sections rather than cylindrical shapes (Blank & Fosberg, 1989; Hamamoto et al., 2016). Quantifying such angular form of pores is not only crucial for a realistic representation of soil microscale structure, but it also has a significant impact on water configuration and soil hydraulic conductivity (Raoof & Hassanizadeh, 2012). For instance, using fast tomography imaging in simplified porous media made of packing of glass beads and in sands, Hoogland et al. (2016) characterized corner flow and conductivity dynamics during soil drainage process. As pores are drained or dried, a fraction of water remained in the pores' angular corner (Tuller et al., 1999). Many studies have shown that the assumption of cylindrical pore cross-section that only allows for single-phase occupancy was insufficient to represent water configuration and hydraulic continuity (Zhou et al., 2000; Tuller & Or, 2001). On the other hand, angular pores allow retaining two or more fluids simultaneously and thus better represent liquid configuration in soil. Joekar Niasar et al. (2009) developed a geometry-based approach for pore network modelling to characterize and produce various ranges of pore cross-sections to describe natural pore geometry, including irregular hyperbolic triangles and regular hyperbolic polygons. The pore geometry and angularity are also essential factors controlling colloid and microbial transport in unsaturated soil (Bradford & Torkzaban, 2008; Saiers & Lenhart, 2003). For instance, Ebrahimi and Or (2014) showed that pore angularity impacts effective water film thickness necessary for bacterial motility in unsaturated soil. In addition, soil macropores and their orientation are known to significantly impact hydraulic conductivity by allowing the rapid flow of water in the soil. Micropores are created by worm holes, plant roots, soil aggregation, and soil wetting/drying. Recent advances using X-ray CT imaging allowed for characterization and quantification of such soil pores at higher resolution compared to traditional methods that used dye tracing, spectral image analysis, and sectioning soil into thin layers (Katuwal et al., 2015; Li et al., 2016; Hu et al., 2020). It is worth mentioning that as with all imaging and image-based techniques, there is a constant temptation to include more and more detail on different physical processes into models. Novel technologies provide a detailed view of soil pore structure

Fig. 11.2 (continued) decreasing sizes, with larger balls ranked as ancestors and small ones as daughters, the identification of common element between families (bonds between pores), and the assignment of geometrical properties to the bonds identified (e.g., angularity, surface area, shape factors). Further details of the substeps required by the morphological and irregular pore network approaches can be found in Table S11.1
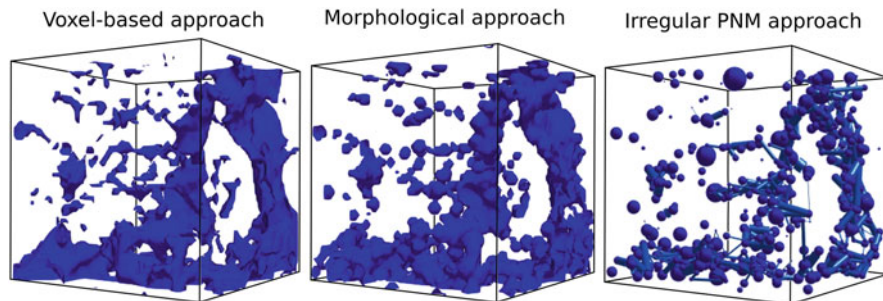
Voxel-based approach   Morphological approach   Irregular PNM approach

Fig. 11.3 3-D view of a pore geometry integrated in the voxel-based, morphological, and PNM approaches. In the morphological approach, balls are used as geometric primitives. In the irregular PNM approach, cylindrical bonds are used. The size of the ROI is 56x56x56 voxels. The voxel resolution is 9.77 μm (Peth et al., 2014)

however, the challenge remains in finding the right balance in terms of the number of measurable details that need to be captured in the models and observations to effectively describe soil function while reducing the inherent complexity of soil. Not all details matter but direct simulation alone or in combination with homogenization approaches (discussed later) is needed to determine which features matter and when; this process allows for systematic classification of processes/phenomena into important and unimportant functional traits.

The advantage of morphological models and irregular PNMs is that they provide a close approximation of the X-ray CT image-based soil pore space as they retain the spatial heterogeneity of the clustering of pores and connectivity in addition to the pore-size distribution (Blunt, 2001; Xiong et al., 2016; Perez-Reche et al., 2012). These methods compact the data information provided by the X-ray CT images and represent an interesting alternative to estimate soil processes in larger-scale simulations than can do the voxel-based models.

As an illustrative example, we have used a set of synchrotron X-ray CT images of soil aggregates from Peth et al. (2014) to show how pore space is integrated in three selected image-based model approaches: a lattice-Boltzmann Method (LBM), a morphological model, and an irregular PNM. Before segmenting the image, we reduced the noise of the image using a non-local filter mean and passed an unsharp mask to enhance contrast between phases (Schlüter et al., 2014). We then applied a local segmentation using a watershed algorithm (Marker-Controlled Watershed in MorpholibJ plugin of Fiji/ImageJ, Legland et al., 2016) to obtain a binary image, with white voxels corresponding to the solid phase and black voxels corresponding to the pore phase. Post-processing of the binary image was further performed with a majority filter to remove segmentation noise. The segmented image was then integrated in the LBM which is a voxel-based model by making a direct correspondence between each X-ray CT voxels and the nodes of the model numerical grid. The same segmented image was then integrated in the morphological model of Monga et al. (2014) and the irregular PNM of Ebrahimi et al. (2013). Figure 11.3 displays the same region of interest (ROI) of the image to better highlight the differences in
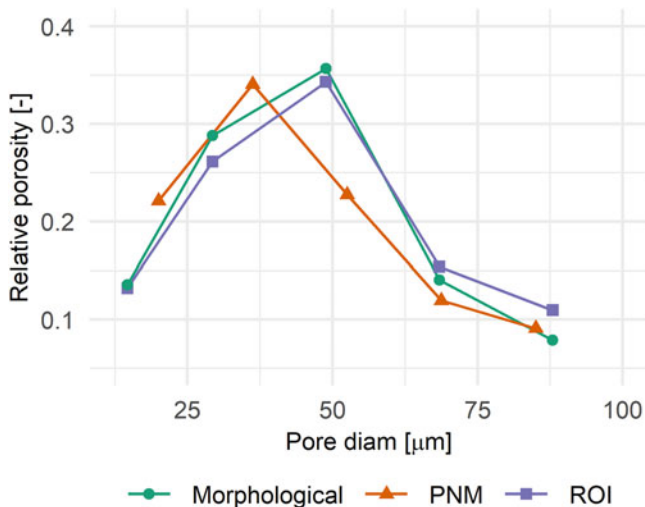
Fig. 11.4 Pore-size distribution of the ROI (56×56×56 voxels) of Peth et al. (2014) image, obtained with a voxel-based (purple), morphological (green), and the irregular PNM (orange) depicted in Fig. 11.3

pore space recovering by the three approaches. The porosity obtained with the three approaches was 0.1233, 0.1054, and 0.0986 for the voxel-based, morphological, and irregular PNM approaches, respectively. Comparison of the pore-size distribution obtained with the three methods can be seen in Fig. 11.4. A priori, underestimations of the pore space volume recovered by the irregular PNM and morphological model can be expected due to the approximations these methods assume. Nonetheless, for this image, these approximations did not translate into a substantial loss of the pore-size classes of the pore volume. The morphological approach, which consists of a minimal set of maximal balls that barely overlap, reproduced the pore-size distribution of the ROI computed with the morphological opening released in the MorpholibJ plugin of Fiji/ImageJ (Legland et al., 2016) well. The slight underestimation of pore volume in PNM is associated with the throat assignment step in which the neighbouring maximal balls to a pore are converted to a throat with a constant size. The throat size is chosen based on the average size of maximal balls connecting two pores that tends to overrepresent small balls.

11.2.2 Integration of X-ray CT Data of Air–Water Distribution

The fact that attenuation of X-rays by water is comparable to that of organic matter hinders distinguishing these two phases in soil X-ray CT images. Imaging protocols are not always straightforward (e.g., Rezanezhad et al. (2010) did not distinguish water from organic matrix of peat soils). In the case of peat soils, distinguishing water from organic matrix relies on the equilibration time between peat and water, which results in some solutes being incorporated to the water surrounding peat, blurring the distinction between phases. If water in the saturated peat is replaced with deionized water, contrast is enhanced and distinction of the two phases is possible (Iain Young, personal communication). High quality images and a resolution targeted to the visualization of air–water interfaces in well resolved pores are thus required. For instance, air-filled and water-filled pores were successfully segmented in X-ray CT images of soil columns (e.g., Mooney, 2002; Daly et al., 2015). Imaging the spatial distribution of water and air phases in the soil pore space can be more easily measured using synchrotron radiation X-ray CT (e.g., Carminati et al., 2008; Pot et al., 2015; Daly et al., 2017). Another option is to stain water by heavy contrast agents. Li and Tang (2019) used an iodine-based contrast medium to visualize water films in glass beads and sand, but they could not observe them in a clayey soil. Our previous experiences have shown that the drawback of using contrast agents, particularly in structured clayey soils, is the massive change in electrolyte concentration in the soil solution brought by adding contrast agent solution (such as KI), which could lead to strong soil dispersion (Pot et al., 2011). Scotson et al. (2019) investigated the use of gold nanoparticles for X-ray CT contrast enhancement, which might well provide a promising avenue, especially for soil biological processes, as gold is inert.

The water distribution and movement can be more easily measured using neutron imaging. Neutrons interact strongly with light elements such as hydrogen allowing for better distinction of soil water at the expense of a poorer representation of soil minerals. Combining X-ray and Neutron CT images using data registration techniques allows exploiting this complementarity and obtaining the solid, air, and water phase distributions experimentally (Clark et al., 2019). This process requires de-resolving the higher resolution image (usually X-ray CT) to match the lower resolution data, which can be done, for instance using Fiji/ImageJ. Despite that in principle, the whole range of soil water content can be resolved, the accuracy is largely influenced by the spatial and temporal resolution achievable by the tomographic method (Tötzke et al., 2021). For instance, Moradi et al. (2011) reported rhizosphere volumetric water content profiles of a sandy soil sieved to <2 mm that ranged from 0.05 to 0.4, approximately.

To date, only a few image-based models have integrated X-ray CT imaging of water and air distributions directly (Keyes et al., 2013; Daly et al., 2015, 2016). Rather, these distributions have been computed using drainage and imbibition algorithms that calculate the typical capillary pressure head that allows air or water
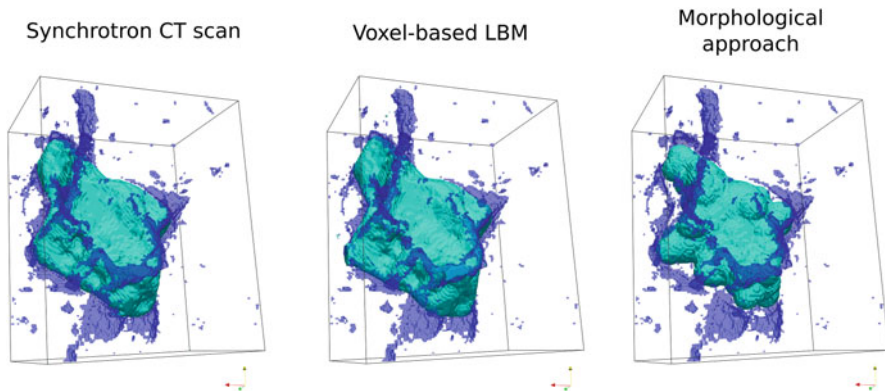
Synchrotron CT scan   Voxel-based LBM   Morphological
                                                       approach

Fig. 11.5 Images of air–water interfaces in a disturbed soil sample, as measured by synchrotron X-ray CT imaging and as produced by a voxel-based approach and a morphological model (Pot et al., 2015). Cyan is the iso-contour of the air–water interface and dark blue is the liquid phase

invasion in the pore network. The sequence of pore invasion by air or water is determined by pore size and pore connectivity only and ignoring the viscous effects and gravity. In the case of drainage, the network of pores is initially assumed to be water filled. Then pores connected to the network entry or already invaded neighbouring pores are drained in a sequence of decreasing pore size. Each pore is evaluated for air invasion based on its size and experienced pressure head according to the Young–Laplace equation. This is adopted in modelling frameworks using morphological models and PNMs (e.g., Carminati et al., 2008; Monga et al., 2014; Ebrahimi & Or, 2015; Pot et al., 2015; Hoogland et al., 2016; Kemgue et al., 2019). Another option is to apply interfacial (van der Waals) and capillary forces to the simulated fluid to generate a phase separation between regions of high fluid density and low fluid density, respectively, attributed to water and air. This approach is adopted in the voxel-based LBM (e.g., Falconer et al., 2012; Genty & Pot, 2013) and in finite-element solvers such as the commercial software COMSOL Multiphysics (Cooper et al., 2017, 2018). LBM solvers with free licenses for research such as PALABOS (Latt et al., 2021) and DL_MESO (Seaton et al., 2013) are available. When interfacial and capillary forces are computed there is a remarkable agreement of the position of the air–water menisci to that measured in X-ray CT images (Pot et al., 2015). Good agreement can also be obtained using morphological models and PNMs (Carminati et al., 2008; Pot et al., 2015) even if the air–water interface presents as an abstracted geometry of the real pore space using Euclidean geometries with defined angularities (Hoogland et al., 2016).

The success of numerical methods to compute water and air distributions in pore space geometries extracted from X-ray CT images and the difficulty in obtaining X-ray CT imaging of water and air distribution in complex soil samples explain the wide adoption of these methods. As an example, Fig. 11.5 displays a comparison between synchrotron X-ray CT imaging and air–water interfaces computed using the LBM and the morphological approach. The mean absolute error between simulations

and measurements of the position of the menisci were 5% and 18% for the LBM and morphological approach, respectively. As can be seen in the picture, performance of the methods is remarkable, especially for the LBM approach.

11.2.3 Integration of X-ray CT Data of Solid Organic Matter Distribution

The similar attenuation of X-rays by water and solid organic matter also hinders the imaging of soil organic matter in X-ray CT images (see Chap. 10). However, large fragments of organic matter, the particulate organic matter (POM), can be rather easily visually identified due to their recognizable shape, as was shown when comparing X-ray CT with micromorphological study of organo-mineral assemblages in thin sections (Elyeznasni et al., 2012). Multi-modal segmentation tools can be used to correctly segment POM and avoid false coatings of organic matter around large pores, due to partial volume effect (e.g., Elyeznasni et al., 2012; Schlüter et al., 2014). However, the identification of small organic matter embedded in the soil matrix remains a challenge and needs the adoption of organic matter staining (Peth et al., 2014; Van Loo et al., 2014; Quigley et al., 2018; Piccoli et al., 2019a; Zheng et al., 2020; Maenhout et al., 2021). Despite that some measured X-ray CT organic matter distributions are available in the literature, this information has not been used in modelling studies yet. Instead, scenarios of organic matter placements in the segmented X-ray CT images have been used (e.g., Falconer et al., 2015; Portell et al., 2018).

To initiate integration of realistic 3-D X-ray CT images of spatial distribution of organic matter, we take the example of the soil image obtained by Peth et al. (2014) that we partially displayed in Fig. 11.3 and extracted the structural information required by image-based modelling (Fig. 11.6). Peth et al. (2014) irreversibly fixed osmium to the organic compounds of the soil. To locate the stained organic matter, the soil sample was scanned at a synchrotron at two photon energies above and below the absorption edge of X-ray by osmium. To obtain Fig. 11.6, we first applied a noise reduction pre-processing on both images, using a median 3-D filter and passed an unsharp mask to enhance contrast between phases (Schlüter et al., 2014). Following the procedure in Peth et al. (2014), we subtracted these images and obtained a 3-D image where the highest grey levels correspond to the highest concentrations of osmium associated with large fragments of organic matter (POM) and lower grey levels correspond to organic matter coatings of pore walls or organic matter residing in smaller pores within the soil matrix (Peth et al., 2014). A global segmentation using three thresholds whose values were initially chosen using Otsu and C-means segmentation algorithms was carried out. This resulted in a multi-modal image where the three types of organic matter identified in Peth et al. (2014), associated to different levels of osmium concentration, were distinguished. A majority filter was passed on the resulting image to remove noise associated with
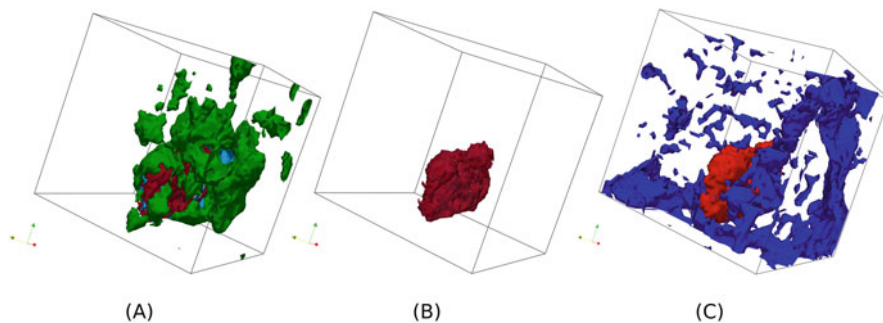
Fig. 11.6 3-D views of soil fragment showing osmium-stained soil organic matter. (**a**) Total organic matter with high (red), medium (cyan), and low (green) relative osmium concentration, (**b**) Piece of organic matter showing a high relative osmium concentration, (**c**) Pore phase (dark blue) and the same organic matter stained with a high relative osmium concentration. The size of the ROI is 56×56×56 voxels. The voxel resolution is 9.77 μm (Peth et al., 2014)

the segmentation step. To integrate this structural information on organic matter in an image-based model, we merged this information with the former binary image containing information on the pore and solid phase as discussed in sect. 11.2.1. To do so we simply added both images to get a multi-modal image. This structural information can now be directly integrated in an image-based model, e.g., the lattice-Boltzmann model of Pot et al. (2010), where different reactivity of the solid–pore interface is included.

11.2.4   Integration of X-ray CT Data of Roots

Despite the recent popularity for rhizosphere related research, few rhizosphere image-based modelling approaches are available to date, probably due to the rhizosphere complexity (both in terms of processes and soil phases involved) and to the challenges faced by the structural imaging of plant–soil interactions such as the identification of soil phases and difficulty of imaging fluxes (see Roose et al., 2016). Distinction among root and other soil phases is increasingly being performed yet it remains challenging, suffering from the limitations such as partial volume effects already highlighted previously. For instance, the pioneering work of Keyes et al. (2013) used Synchrotron X-ray CT and successfully identified root hairs, soil, pore space, and root surface regions. Also, along with the characterization of mucilage and root hairs, and water sorption of chickpea roots, Rabbi et al. (2018) computed the radial and axial water permeability using lattice-Boltzmann modelling based on X-ray CT images of sieved and repacked soil. Given that they are usually filled with water, roots can also be identified using neutrons. For instance, Zarebanadkouki et al. (2012, 2014) used neutron radiography to visualize the transport of deuterated water and developed a method to reconstruct flow into roots. Segmentation of the

reconstructed images is complex, often involving semiautomatic methods (Keyes et al., 2013; Daly et al., 2016). Open-source semiautomated tools to follow root growth such as RooTrak (Mairhofer et al., 2016) or the Fiji/ImageJ plugin Smart Root (Lobet et al., 2011) as well as commercial tools such as WinRHIZO are available (see Chap. 9).

Once segmented, the root structural information is used to set up the processes of interest. To date, the most studied processes are nutrient uptake (mainly P), uptake of water in saturated and unsaturated conditions, and root growth. Unlike root architecture-based approaches, which use volumetric reactions/uptake terms, spatially explicit image-based approaches use the root structural information to define the boundary conditions suitable to the process of interest (Ruiz et al., 2020b). Keyes et al. (2013) used Michaelis–Menten nutrient uptake conditions to simulate P uptake by root and root hairs. McKay Fletcher et al. (2019) also assumed a Michaelis–Menten nutrient uptake boundary condition on all active roots but added a constant citrate exudation rate per surface on root tips to study organic-acid enhanced P uptake. Daly et al. (2018) assumed a water uptake rate proportional to the radial conductivity of water through root epidermis and the pressure drop between root internal xylem pressure and the water soil potential. The internal xylem pressure adopted was 1 MPa during the day and 0 MPa at night. For an in-depth explanation of the mathematical expressions adopted by current approaches, readers are referred to the reviews of Ruiz et al., (2020b) and Daly et al. (2016). So far, assumptions about the specific uptake/exudation regions need to be tackled using expert knowledge due to the lack of structurally explicit data. Root (or root hair) growth is currently being studied using time-dependent boundary conditions. A common technique to do so is assuming a given geometry and activating the appropriate boundary condition according to a (measured) growth rate (e.g., McKay Fletcher et al., 2020). In this approach, the developed root segment is used, but the uptake/exudation properties are activated at the appropriate time after having started the simulation.

11.3 Overview of Image-Based Modelling Works

11.3.1 Modelling of Soil Physical Processes

11.3.1.1 Saturated Water Conditions

The macroscopic properties of transport in soils depend on the 3-D organization of the pores and their size (Dullien, 1992). In that regard, the direct integration into transport models of X-ray CT images accurately describing soil cavities and their connectivity is a unique opportunity to explain soil hydrodynamic properties. Several works have numerically calculated 3-D water velocity fields in X-ray CT images of soil samples (e.g., Daly et al., 2015; Dal Ferro et al., 2015; Pot et al., 2020; Zhang et al., 2021a). To carry out image-based modelling, the images are segmented into

binary information representing the soil pores and the solid phase (see Sect. 11.2.1). Mathematically, rigorous up-scaling for fluid flow computation, where Darcy's law is derived from Stokes' equations solved at the microscopic scale (Daly & Roose, 2014), enables the calculation of the hydraulic conductivity and soil water retention curve, based on a representative element volume (REV)(see Chap.3). The periodicity of the soil architecture of the REV is also required. However, the search for an image size that is representative of the physical properties of the soil such as porosity and/or hydraulic conductivity has been rarely carried out (Daly et al., 2015; Gharedaghloo et al., 2018; Gerke & Karsanina, 2020). In other cases, the aim is to understand how flow paths emerge in the complex pore space (e.g., Pot et al., 2020) and how the macroscopic property of interest (calculated at the ROI scale), such as permeability, emerges from the 3-D water velocity fields calculated at the microscopic scale (pore organization within the ROI, e.g., Menon et al., 2011; Deurer et al., 2012; Khan et al., 2012; Zhang et al., 2021b).

In almost all the studies above, the voxels of the segmented image were directly mapped to grid nodes and the Stokes' water flow was computed in the complex pore geometry using either the Lattice-Boltzmann approach (Menon et al., 2011, 2015; Hyväluoma et al., 2012; Zhou et al., 2018; Pot et al., 2020; Zhang et al., 2021b), finite-element solvers (e.g., Daly et al., 2015, 2017; Gerke et al., 2018; Gerke & Karsanina, 2020) or a finite-volume solver (Gackiewicz et al., 2019). Other approaches such as smoothed particle hydrodynamics (Dal Ferro et al., 2015) have also been used. Gharedaghloo et al. (2018) assumed an irregular PNM model. The network of pores extracted from segmented X-ray CT images consisted of cylindrical throats and volumeless nodes (see Sect. 11.2.1) and the water flow through the throats was calculated by solving a system of linear water balance equations (Valvatne & Blunt, 2004). To carry out the flow calculation, periodic conditions at the edge of the images are applied and a pressure gradient or force field (gravity) imposed. Once the steady state is reached, the 3-D water velocity field, which is the velocity at each node of the computational grid, is saved. Visualization of these 3-D fields reveals preferential flow paths. As a matter of example, visualization and characterization of flow pathways evidenced that pores of similar size contributed unequally to flow resistance in biological crusts (Menon et al., 2011). This work also provided qualitative insights on soil surface seal functioning by showing how only a few flow channels penetrated through the surface seal and revealed strong lateral flows below these seal structures (Hyväluoma et al., 2012). Permeability (or saturated hydraulic conductivity) is then calculated by integrating the 3-D fluid velocity fields over the ROI. In that respect, image-based modelling outputs have highlighted the major role that large conductive pores have on water flow (e.g., Dal Ferro et al., 2015). They have also confirmed that: (i) variability in permeability is largely affected by size and by a few key pore throats (e.g., Gharedaghloo et al., 2018; Pot et al., 2020; Zhang et al., 2021a) and (ii) that porosity is not the sole morphological parameter explaining such permeability, suggesting that pore-size distribution and the pore network connectivity and tortuosity must be considered as well (e.g., Zhou et al., 2018).

The outputs of image-based models have also been compared to X-ray CT-derived pore space morphological parameters such as porosity, pore-size distribution, connectivity (Euler number), tortuosity, and critical diameter of the percolating pores. Many of these parameters can already be calculated with existing open-source free image analysis software (e.g., Fiji/ImageJ, QuantIm), while others, including tortuosity, remain more complicated to obtain (e.g., Gommes et al., 2009; Roque & Costa, 2020). Tortuosity can be estimated from spectral dimension (e.g., Crawford et al., 1993) or by computed 3-D fluid velocity fields or solute diffusion fields in 3-D images (e.g., Koponen et al., 1996; Berg & Held, 2016; Zhang et al., 2021b). Correlations between these morphological parameters and outputs of the image-based models are commonly investigated in the literature. For instance, prediction of a reduction of flow rate when biological crusts and repacked soil aggregates are submitted to compaction was related not only to the reduction in total porosity but also to a modified pore-size distribution (Menon et al., 2011, 2015).

In an alternative indirect approach, X-ray CT images are first analysed to deliver morphological parameters such as the ones described above. These parameters are subsequently used in macroscopic empirical models that predict water content, hydraulic conductivity, and solute diffusivity. Examples of these empirical models are the well-known empirical Kozeny–Carman equation and other relations based on percolation theory and critical path analysis (Katz & Thompson, 1986) which relate the saturated hydraulic conductivity with specific surface area, tortuosity, and a characteristic length of the pore size. As found in works dealing with porous rocks (e.g., Nishiyama & Yokoyama, 2017), this indirect integration of 3-D X-ray CT data of soils has allowed to demonstrate that the critical path diameter is a better parameter to be used in the Kozeny–Carman equation as compared to the mean hydraulic radius (Koestel et al., 2018; Pot et al., 2020). Luo and Lin (2009) used X-ray CT imaging to show that fractal dimension alone was insufficient to characterize soil macropore structure and flow patterns including a lacunarity function that reflects size distribution of macropores as a diagnostic value to better describe soil structural properties. Packages included in existing image analysis software can also be used to compute diffusion processes. The QuantIm software (Vogel, 2008) solves Fick's law of diffusion in 3-D with a finite difference approach. Using this package, Deurer et al. (2012) calculated the apparent diffusion coefficient of macropore networks around soil aggregates. They extracted small ROIs from segmented X-ray CT images of soil cores sampled under tree-rows and wheel-tracks and computed the diffusive flux within them. The size of the ROI was chosen to encompass a sufficiently large number of soil aggregates (almost 100). They attributed the absence of significant differences in the gas diffusion coefficient between ROIs to the similarity in the volume of pores larger than 1 mm and to the fact that they were well connected. Lattice-Boltzmann model (Zhou et al., 2019) and PNM (Gharedaghloo et al., 2018) were also used to compute solute transport properties. According to theory of transport in porous media, Zhou et al. (2019) predicted an increase of the solute dispersion coefficient in soil macroaggregates amended with biochar resulting from an increased saturated hydraulic conductivity. For peat soils,

the diffusion coefficient decreased with depth driven by an increased tortuosity whereas dispersivity did not vary considerably (Gharedaghloo et al., 2018).

11.3.1.2   Unsaturated Water Conditions

Soil water movement has been modelled classically using Richards' equation, which consists of a mass conservation combined with two equilibrium measurements for the partially saturated hydraulic conductivity and soil suction characteristic that relates the level of relative soil saturation to the soil water pore pressure. As such, both measurements can take a long time and hence the need for intelligent estimation of these values based on various morphological and textural information. In addition, both hydraulic conductivity and suction characteristic exhibit hysteresis, i.e., the shape of the curve as a function of saturation is different depending on if the measurement is done whilst drying or wetting the sample. Currently, this compounds the problem for measurements as to capture the hysteresis one would need to be doing numerous long wetting and drying experiments (weeks and months) very accurately so the locations of the Haine's jumps are accurately captured for hysteresis; not to mention the extra sets to capture scanning curves between the wetting and drying at the intermediate points. Nonetheless, as suggested by Berg et al. (2013), who were able to directly image Haine's jumps in sandstone samples using X-ray CT, future developments may allow to speed up the process.

Currently, Haine's jumps can be predicted using modelling. The mathematical foundations for this that were used on X-ray CT images were established by Daly and Roose (2015). Cooper et al. (2018) expanded the previous work of Daly and Roose (2015) and Cooper et al. (2017) to include the effect of plant exudates on the water release curve (and hence Haine's jumps) and the hydraulic conductivity. We next discuss how this was undertaken by giving a flavour of mathematical analysis involved.

We have already discussed above the ways X-ray CT measurements can be used to capture some of the statistics for estimating saturated hydraulic conductivity. An essentially similar approach can be employed to capture the partially saturated hydraulic conductivity curves if one scans the soil samples whilst wetting and drying and segments out the water–mineral and water–air interfaces. However, this is a very intensive image analysis endeavour. Rather, it would be much better to be able to predict computationally in combination with soil pore space imaging how the wetting and drying influence partially saturated hydraulic conductivity and soil suction characteristics. The fundamental science/mathematics concerning this was established by Daly and Roose (2014, 2015) and implemented directly on images by Cooper et al. (2017) and expanded to include root exudates that change the water wetting and drying properties in the pore space by Cooper et al. (2018). All this work was possible due to the rigorous application of the homogenization theory. Homogenization theory is a perturbation approach which assumes that a composite material, i.e., soil in this case, is comprised of many small things. This means that there is a microscale x and macroscale y and that the ratio of the two $x/y = \varepsilon$ is small. The next

step in homogenization assumes that the solution depends on each of these independently and upon application of the perturbation in ε, a sequence of analytic mathematical problems can be found that determine what microscale features matter at the macroscopic scale. For example, after Daly and Roose (2014, 2015) and Cooper et al. (2017, 2018), this approach gave a computational analytic approach to calculating partially the saturated hydraulic conductivity tensor and soil suction characteristic, including wetting and drying Haine's jumps, based on the images of the pore space.

Constrained by the intensive image analysis tasks involved, very few works have attempted to use successive X-ray CT scans of soil samples at different water contents. Using an indirect integration of X-ray CT data, Rezanezhad et al. (2009, 2010) proposed a modified Kozeny–Carman equation taking into account the soil air-filled porosity. The parameters of the air-filled fraction were extracted from X-ray CT images of peat soils scanned at different water contents. Reasonably good agreement was obtained between the predicted conductivity and the experimentally measured one. The increasing number, volume, and tortuosity of the air-filled pores imaged were key parameters in these organic soils to explain the decrease of the unsaturated hydraulic conductivity. Fast scanning X-ray CT data of soil columns subjected to rainfall infiltration were also used to extract two key parameters to be used in a 1-D macroscopic preferential water flow model coupling a soil-matrix capillary flow and a gravity-driven macropore flow: the percolating macroporosity and the characteristic size of the porous medium, which was defined as the average half-distance between percolating macropores (Lissy et al., 2020). The latter parameter controls the lateral flow from macropores to soil matrix and was calculated using a Voronoï diagram of the X-ray CT image. Fixing these parameter values in the model strongly improved the mechanistic understanding of water exchanges between macropores and soil matrix. In particular, as it could be expected, the model was able to generate large water exchanges between macropores and the soil matrix for initially drier soil conditions.

Indirect integration of X-ray CT data has also been used to compute the partially saturated hydraulic conductivity and the soil suction characteristic. Knowledge of the pore-size distribution was delivered by 3-D X-ray CT imaging and the water release curve was calculated from it using the Young–Laplace equation (Beckers et al., 2014). Computation of the soil hydraulic function was subsequently carried out using the macroscopic numerical unimodal (van Genuchten, 1980) and dual porosity (Durner, 1994) models calibrated with the water release curve predicted from the pore-size distribution. The addition of supplementary X-ray CT-image-based data in the water retention curve allowed an improved calibration of the dual porosity model and enhanced predictions of the near-saturated hydraulic function.

Pore-scale imaging can also be used to characterize fractal geometry of pore space and water distribution with implications to determine gas transport and permeability of porous media (Yu & Liu, 2004; Liu et al., 2019; Piccoli et al., 2019b; San José Martínez et al., 2010). For instance, Liu et al. (2019) used X-ray CT imaging to show that the water and gas distributions of quartzitic sands are fractal. Using an indirect approach, they extracted the area and tortuosity fractal

dimensions from X-ray CT images in order to develop a fractal theory-based relative permeability model to describe water and gas distributions in pores. Others have developed a number of fractal based models to describe soil unsaturated hydraulic conductivity using a fractal model for the water retention curve and the pore-size distributions (Tyler & Wheatcraft, 1990; Xu, 2004; Alfaro Soto et al., 2017; Ghanbarian & Hunt, 2017).

X-ray CT image-based information has also been indirectly integrated into 3-D macroscopic numerical models of water and solute transport. Unlike a direct integration, a computation mesh covering the whole domain, not only the pore space, is generated in this approach. Values of the parameters of the water release curve and hydraulic conductivity function are locally calculated as a function of either the type of material (denser regions defined as high grey values of the X-ray CT image and less dense regions defined as low grey values, Kasteel et al., 2000) or as a function of the local porosity obtained after segmentation of the X-ray CT images (Dohnal et al., 2013). These studies confirmed that solute spreading simulated at the column scale was sensitive to the difference in the local saturated hydraulic conductivity but not to the local dispersivities (Kasteel et al., 2000). Additionally, Dohnal et al. (2013) complemented X-ray CT data with 3-D data of water content obtained by Magnetic Resonance Imaging (MRI) to determine maps of entrapped air that was added to the 3-D macroscopic model as no-flow regions. Their modelling results supported the assumption that the observed decrease in outflow rate during repeated infiltration experiments could be caused by entrapped air in large pores. Moreover, the spatial distribution of the entrapped air had a greater impact than its volume.

Comparing predictions of an image-based model relying on accurate representations of 3-D air–water interfaces to long established semi-empirical equations from experimental determinations was used to better understand solute transport in unsaturated conditions (Genty & Pot, 2014). At the same time, this allowed testing the robustness of the direct image-based models used. Genty and Pot (2014) integrate X-ray CT pore geometries in an image-based model that computes the phase field equation (described in Sect. 11.2.2) obtaining explicit air–water interfaces at different water contents and at equilibrium. The air–water distributions were subsequently used by a second image-based model of solute transport. The 3-D solute diffusion fields at specific water contents produced by this second model allowed the estimation of the effective diffusion coefficient at the scale of the ROI through an inversion of a macroscopic analytical solution of the Fick's law. A good agreement with the macroscopic semi-empirical equation based on Archie's law, which relates the effective solute diffusion coefficient and the water saturation, confirmed the classic value of the exponent of Archie's law used for soils (Genty & Pot, 2014). Hu et al. (2018) also used knowledge of equilibrated air and water distributions, this time calculated by a morphological image-based approach, and directly integrated this 3-D structural information in a simplified free-surface model considering static equilibrium to predict unsaturated water flow.

The final approach to simulating the unsaturated fluid flow in soils found in the literature is based on an indirect use of X-ray CT data to generate simpler spatially explicit models where the soil processes of interest are subsequently simulated. This

was first done by Vogel and Roth (2001), who integrated soil pore-size distribution and topology data on the pore connectivity obtained from a 3-D reconstruction of serial thin sections of soil to produce a large number of equivalent pore networks, using a regular PNM. These authors demonstrated that this structural information was sufficient to predict the soil suction characteristic and hydraulic properties. Later, Köhne et al. (2011) applied the procedure described by Vogel and Roth (2001) to obtain an equivalent pore network based on X-ray CT images of two arable soils. It is worth noting that these works are following an indirect approach to the integration of X-ray CT data. Unlike irregular PNMs, regular PNMs are generated using regular assemblies of nodes interconnected by bonds of simplified geometry (e.g., cylinders). The length, radius, and number of bonds per nodes are parameters of the PNM. The modelled architecture reproduces an equivalent pore network of similar physical properties of given soil samples such as the pore geometry, size distribution, and degree of connectivity, which are extracted after image analysis of the target X-ray CT data.

11.3.2 Modelling of Biological Processes

11.3.2.1 Modelling of Microbial Activity

Image-based models are progressively moving towards the inclusion of soil biological activity, including fungal (e.g., Falconer et al., 2007), roots (e.g., Keyes et al., 2013), and bacterial (e.g., Vogel et al., 2015) processes, as it has been reported in recent reviews (Roose et al., 2016; König et al., 2020; Golparvar et al., 2021). Image-based modelling of soil microbial activity has essentially emphasized the role of soil architecture in establishing diverse spatial accessibility of organic substrates to decomposers that explain the spatial distribution and growth of fungi (Falconer et al., 2007, 2012, 2015; Pajor et al., 2010; Kravchenko et al., 2011; Cazelles et al., 2013), the bacterial diversity (Portell et al., 2018), and the microbial functions such as the decomposition of organic matter and CO_2 emissions (Ngom et al., 2011; Vogel et al., 2015, 2018; Monga et al., 2008, 2014). For instance, X-ray CT images of undisturbed sandy loam soil were directly integrated in an image-based model of fungal growth dynamics by Falconer et al. (2012). These authors simulated fungal biomass spreading in an X-ray CT pore space directly integrated in the numerical grid of the model. Fungal mycelia biomass was conceptualized by three biomass fractions: insulated (i.e., old inactive biomass), non-insulated biomass (i.e., active hyphal tips), and mobile (i.e., internal translocating resource) biomasses. Insulated biomass is immobile while non-insulated biomass and the internal resource spread through a diffusion process constrained by the pore space and existing fungal biomass subdomains, respectively. The system of partial differential equations was solved using the classical Crank-Nicholson scheme. Local fungal spread was modulated by a diffusion coefficient that is a function of the water content present in the numerical grid.

The water content of the grid elements was computed by an LBM approach (as described in Sect. 11.2.2) implemented in the open-source PALABOS (Latt et al., 2021). Falconer et al. (2012) predicted a significant decrease in fungal growth by increased water saturation conditions. Water-filled pores alter the connectivity of the air phase, which slows down fungal colonization in line with the model assumptions. Nonetheless, the explicit integration of the 3-D distribution of air-water phases in the model suggested that it is the spatial location of water-filled pores rather than the water content itself that is responsible of this loss of connectivity and, therefore, that the bulk water content of the soil samples is insufficient to predict fungal growth and spatial expansion.

The explicit soil architecture imaged with X-ray CT can also be used to study survival and coexistence of different bacterial species in soil. Survival and coexistence of different bacterial species in simplified porous media have been shown to be controlled by the connectivity of the pores, the water saturation conditions, and the respective locations of the nutrients and bacteria (e.g., Long & Or, 2005; Ebrahimi & Or, 2015). As an example, Portell et al. (2018) investigated the role of soil architecture and location of organic matter in the coexistence of three bacterial strains showing competitive, generalist, and poorly competitive profiles. To do so, X-ray CT data of an undisturbed loamy soil was directly integrated in the numerical grid. The methodology coupled a lattice-Boltzmann model, accounting for the diffusion of dissolved organic carbon through the water phase (Genty & Pot, 2013, 2014), and an individual-based model, accounting for the activity of soil microorganisms. The approach also considers explicitly the distribution of organic matter hydrolysing over time following a first-order kinetic of constant rate. Hydrolysed organic carbon is released into the water phase neighbouring the particulate carbon, if there is any. The water–air distribution in the pore space was computed for three saturation levels (0.25, 0.5, and 1) using an LBM approach (see Sect. 11.2.2) described and parameterized in the literature (Genty & Pot, 2013; Pot et al., 2015). The lack of multimodal data covering the organic matter distribution (see Sect. 11.2.3) and bacteria position was tackled here using simulation scenarios assuming a fixed bulk amount of organic matter initialized as solid fragments. Bacteria were positioned randomly on the interface between the pore and solid face, performing repetitions to account for the uncertainty of this distribution. Portell et al. (2018) predicted large effects of the spatial distribution of organic matter on the strain's distribution but a largely unaffected total microbial biomass evolution. The poorly competitive strain was found to grow to the same extent of the other strains when located near large pieces of organic matter. Nonetheless, the presence of more competitive strains in the same microhabitat prevents the growth of the least competitive strain. These outputs are in agreement with predictions performed using simplified porous media that found that survival and coexistence of different bacterial species are controlled by the connectivity of the pores, the water saturation conditions, and the respective locations of the nutrients and bacteria (e.g., Long & Or, 2005; Ebrahimi & Or, 2015).

Integration of X-ray CT structural information into image-based models allowed the investigation of the role of differentiated soil porous architectures of a silt loam soil either subject to conventional tillage or under a grassland on organic matter

decomposition (Ngom et al., 2011). In this study, the pore space of the segmented X-ray CT data was approached by means of a morphological approach based on spheres (see Sect. 11.2.1). The water retention curve of the ROI was simulated using the Young–Laplace law with a zero-contact angle between water and soil (Sect. 11.2.2). The biological sub-model described in Monga et al. (2008) was then used to simulate organic matter decomposition. This model simulates the growth, respiration, mortality, and dormancy of densities of microorganisms placed in its constituents' maximal balls. To mimic extracellular enzymatic decomposition, the model assumes that soil organic matter within a ball can be decomposed by microorganisms placed in all balls connected through the water-filled path. Organic matter decomposition is modelled assuming an offer/demand approach comparing the maximal decomposable masses (offer) and the maximal microorganisms' needs (demand). When the offer is less than the demand, the former is distributed according to the geodesic distance between the resources and the microorganisms using a polynomial repartition law. Simulation scenarios conducted by Ngom et al. (2011) used a temporal extent of 100 days and distributed organic matter and bacteria in pores of different sizes by placing organic matter in pores smaller than 20 μm and immobile bacteria in larger, more aerated pores. Ngom et al. (2011) suggested that small, isolated pores largely decreased organic matter availability to microbes, hindering mineralization in the conventional tillage treatment, whereas more connected pore space facilitated mineralization of most of the organic matter on the grassland treatment.

In a recent study, the impact of fertilization on the health of microbial communities was tackled using a direct finite-element based approach. This study (Ruiz et al., 2020a) examined how the soil structure and soil moisture content influence nitrogen movements around an ammonium nitrate fertilizer pellet and the subsequent impact on microorganisms' activity. Nitrogen species accounted for in the model are ammonium, nitrate, and dissolved organic nitrogen, which were subjected to the processes of N immobilization, ammonification, nitrification as well as diffusion in the water phase. Samples were imaged with X-ray CT from where the soil phase, air phase, and the fertilizer pellet were segmented. The water distribution in the segmented pore space was computed using a two-phase water–air model (see Sect. 11.2.2). Release of nitrogen to the water phase is modelled using appropriate boundary conditions on the surface of the pellet. Boundary conditions around the soil phase were used to model the sorption and desorption of chemical species as well as chemical transformations mediated by microorganisms. The microbial population size responsible for these transformations was assumed to be fixed for the time length of the simulation. The reduction in the microbial activity due to cytotoxic concentrations of fertilizer was calibrated using preliminary experiments. Ruiz et al. (2020a) found that diffusion and concentration of nitrogen in the water phase is critically dependent upon soil moisture and chemical species considered and provides predictions for the maximum concentrations of ammonium and nitrate around the pellet under dry conditions.

In addition to the direct approach, X-ray CT data has also been indirectly used in modelling studies to understand the consequences of structural heterogeneities in

soil microbial diversity and functioning. For instance, experimental studies have shown that low pore connectivity and heterogeneous water configuration in soil increase microbial diversity (Carson et al., 2010) and interaction (Tecon et al., 2018). Using statistical estimates of pore sizes and distances between interstitial sites obtained from existing X-ray CT images of soil samples, Resat et al. (2012) produced simplified soil aggregate structures with random, continuously-connected pores. They studied the dynamics of microorganisms using two distinct carbon obtention strategies: microorganisms with membrane-associated hydrolase and microorganisms releasing extracellular hydrolases. The authors found that coexistence of both strategies produced higher cellulose utilization efficiency and a reduced stochasticity. They also concluded that bacterial growth dynamics was the result of a balance between the substrate degradation kinetics, the dynamics of enzymes produced by the microorganisms, and the diffusive processes taking place in the modelled pore space. Their modelling work also supports previous evidence that bacteria tended to grow preferentially near the carbon source.

Burrowing activity of soil fauna makes the soil architecture a highly dynamic variable. A realistic consideration of the modification of soil architecture by its biological components is needed as it impacts not only soil microbial functions, but soil physical functions as well. The latter were investigated by Bastardie et al. (2002) who built simplified 3-D networks of earthworm burrows in which they simulated saturated water flow. The networks were made of a series of connected cylinders, which represented segments of earthworm burrow systems. Using an indirect approach, they extracted statistical estimates of length and orientation of these segments from X-ray CT images of a repacked soil core colonized by a single earthworm (Capowiez et al., 1998) to generate a large number of equivalent porous media. Earthworm trajectories were computed by predefined rules of worm movement obtained from experimental observations in 2-D terraria (Capowiez & Belzunces, 2001). Therefore, like regular PNMs, physical properties of these equivalent porous media such as length and orientation of the burrow segments are reproduced but their actual spatial arrangement is disregarded. Bastardie et al. (2002) showed parameters such as the volume of pore space and the interconnectedness of burrows were not relevant to explain the permeability of the porous media. Instead, the connectivity of the burrow systems (i.e., the number of independent paths) was found to be a more relevant parameter. So far, actual representation of temporal modification of soil architecture by earthworms has been undertaken using repeated X-ray CT scanning at a low temporal resolution, mainly to highlight modification caused by the treatment applied (Pagenkemper et al., 2015). Nonetheless, this information has not yet been directly used in a model. Instead, Blanchart et al. (2009) generated fractal soil geometry to investigate the role of earthworm burrowing including ingestion and production of casts in compacting and uncompacting soil using an equivalent porous medium. Along the same line, it is worth reporting modelling studies simulating temporal modification of soil architecture by soil microorganisms in which a simplified arrangement of solid particles on a regular numerical grid has been used by some authors (Crawford et al., 2012;

Ray et al., 2017) to tackle the role of the production of gluing agents by microorganisms in gathering soil particles.

It is worth highlighting the role that image-based modelling of soil microbial activity can play in generating mechanistic knowledge of biologically driven processes in complex environments such as soil. One of the approaches used in that respect is the realization of sensitivity analysis where the soil architecture is explicitly taken into account using X-ray CT data (Cazelles et al., 2013; Vogel et al., 2015, 2018). Water–air distributions in the imaged pore space are then usually computed using image-based modelling for different water contents (see Sect. 11.2.2). Varied organic matter distributions (see Sect. 11.2.3) and positions of microorganisms are additionally considered for conducting simulation scenarios. Far from just being a mathematical exercise, such analysis provides valuable insights into how much soil functions and processes are affected by different soil architectures (provided by X-ray CT) and by changes on further abiotic (amount and distribution of organic matter, moisture content, etc.) and biotic (distribution of microorganisms, growth parameters, etc.) inputs. This allows testing of hypotheses about the role of soil architecture on soil microbial activity by unravelling, for instance, the relative importance of the biotic and abiotic components. As an example, analysing fungal physiological processes, soil architecture, and initial carbon distribution, Cazelles et al. (2013) found the spatial extension of hyphal tips and the fungal biomass yield were highly affected by the fungal physiological parameters associated with the growth and recycling processes. Also, Vogel et al. (2018) found that under low accessibility of organic matter to soil bacteria, conditioned by the local structural heterogeneities in the bacteria micro-habitats, the decomposition of organic matter was no longer dependent on the physiological parameters. A general point related with this kind of analysis is that the model assumptions and limitations need to be properly communicated and understood so the results can be appropriately interpreted.

11.3.2.2 Modelling of Root Processes

The prospective of steering rhizosphere management to boost plant productivity while reducing agrochemicals has attracted much attention of the scientific community, including the development of many rhizosphere models. Nonetheless, the number of image-based models existing to date is still very limited (Ruiz et al., 2020b). If we consider models where the soil architecture is considered explicitly, the list of approaches is even more reduced. Keyes et al. (2013) used Synchrotron X-ray CT and developed a finite-element image-based model of phosphate uptake by wheat roots and root hairs and implemented it in COMSOL. The volume mesh used by the model includes root hairs, soil, root surface, and water defined separately. Different grey levels were used to identify the meshed elements thanks to the high quality of the synchrotron light. Potential heterogeneity on the P transporters along the root was not considered due to the lack of data and uptake properties were assumed to be the same over the surface. These authors found that the root surface

was responsible for a slightly superior P uptake (1%) than the root hairs, despite their closest proximity to the soil surfaces, where most of the phosphate was located. In a follow-up study, Daly et al. (2016) expanded the previous model to include both bulk and rhizosphere soil. The soil near the root (i.e., rhizosphere soil) was explicitly described through the integration of X-ray CT data and surrounded by a large/infinite bulk soil (i.e., away from the root). The latter was achieved with the use of a boundary condition obtained by means of homogenization theory. Root-hair growth was mimicked by considering the structure and a time-dependent uptake boundary condition. The study found that the key criterion for convergence of the P uptake was the size of the rhizosphere region considered.

Further work on P uptake by roots focuses on complexifying the P uptake mechanism but also simplifying the structural description of the soil phase. McKay Fletcher et al. (2020) added the exudation of citrate, which can enhance P uptake and study the effect of root system architecture on organic-acid enhanced P uptake of 12-day-old wheat plants. Time-lapse X-ray CT was used to define the root architectures. Boundary conditions were placed as dictated by the measured X-ray CT structures and growth simulated by activating the appropriate conditions mimicking the X-ray CT root growth measured. The soil volume was identified in the X-ray CT images, but the soil architecture was disregarded and a homogenous soil, including a parameter to account for an approximate volumetric water content, adopted. McKay Fletcher et al. (2019) further evolved the approach to investigate how changes in root system architectures of barley (*Hordeum vulgare*) affect P uptake from a fertilizer pellet. The study elegantly combines modelling, X-ray CT, Scanning Electron Microscopy with Electron Dispersive X-ray Spectroscopy (SEM-EDS), and soil thin sections. As in McKay Fletcher et al. (2020), X-ray CT identified solid, water, and pores were assumed as a single homogeneous volume and modelled using a single finite-element mesh. Appropriate boundary conditions are then placed on the boundaries of the root and fertilizer pellet, which were also identifiable in the X-ray CT images.

Daly et al. (2018) used time resolved X-ray CT and modelling to test the accuracy of spatially averaging the water uptake of young wheat plants grown in pots of 50 mm diameter x 80 mm height. Roots, solid, and pore space were identified in the X-ray CT images. The water–air interfaces were computed by implementing Richards' equation for partially saturated flow parameterized with the water release characteristics and the saturation-dependent hydraulic conductivity measured. A finite-element mesh describing the root surface, the soil architecture, and the air phase was created and model outputs for a number of root systems were compared to the averaged model of Roose and Fowler (2004) to account for the effect of explicitly including the root architecture. Comparison of these approaches for a number of root system architectures and two soil types found less than 2% divergence. Nonetheless, the simplified model could not capture the heterogeneous water distribution seen in the image-based approach. Since Daly et al. (2018) performed a number of image treatments averaging many soil particles, it has been suggested that this may actually be masking some nuances at the pore scale not captured in this study (Ruiz et al., 2020b). A more comprehensive review about the use of image-

based modelling to describe water dynamics in the rhizosphere is provided by Daly et al. (2017).

Landl et al. (2019) simulated the impact of naturally created biopores originated from decayed plant roots and earthworm activity on root growth, soil water flow, and root water uptake. In this work, soil properties are defined at the nodes of regular cubic grids, each having a hydraulic state and soil properties. A soil element (volume) was subsequently defined by the properties of the 8 surrounding nodes. They assumed two regular cubic grids, a coarse grid (1 cm) used to compute water flow and a finer one (0.5 cm) to compute growth development affected by soil local conditions. Biopores were modelled as a soil material with a very low penetration resistance to the roots and assumed to be air-filled, thus, not contributing to the water flow. An X-ray CT image stack (231 μm thick) was initially used to set up the position of the biopores directly. A downgrading procedure involving an initial skeletonization of the X-ray CT data was used to assign biopore voxels to the fine grid. The method was found to produce an increased bioporosity while keeping biopore length densities fairly constant. Model parameters were calibrated via the optimization of the root architecture parameters so that simulated and experimentally observed root length distributions were in agreement with each other. Simulation scenarios with the calibrated model showed biopores sustainedly mitigated transpiration deficits by permitting roots to take up water from deeper soil layers. This was found also when a reduced root water uptake in biopores due to limited root–soil contact was assumed.

Assuming an indirect integration approach, X-ray CT data of root architectures growing in soil can be used to parameterize existing root system models. Root system models are approaches simulating the structure, topology, and 3-D placements of roots. Root growth is simulated assuming a set of rules regarding elongation, branching, and death and a discrete approach defining individual segments of root that may have attributes such as radius, age, or hydraulic properties associated is usually adopted (Schnepf et al., 2020). A set of benchmarks, including reference calibration data sets, have recently been proposed by Schnepf et al. (2020), which suggest that methodologies may converge in the near future. As a matter of example of the methodology, Landl et al. (2021) coupled a 3-D root architecture with a rhizodeposition model that accounts for the transport of rhizodeposition. The coupled model is used to investigate spatio-temporal distribution patterns of citrate and mucilage in soil. Root system architectures of *Vicia faba* and *Zea mays* were extracted from X-ray CT images and saved as Root System Markup Language (Lobet et al., 2015). An in-house computer code was then used to extract the model parameters of the root architecture model (e.g., internodal distance, root radius, branching angle, maximal root length). Soil architecture was not explicitly accounted for in this approach. After running a number of simulation scenarios, Landl et al. (2021) found that: (i) rhizodeposition hotspot volumes around roots reached maximum values at intermediate root growth rates, (ii) root branching led to an increased volume of rhizodeposition hotspot zones due to the rhizosphere of individual roots overlapping, and (iii) that the rhizodeposition hotspot values were

smaller around the *Zea mays* root system as compared to the one predicted by *Vicia faba*.

11.4   Conclusions

Whether direct or indirect, the combination of X-ray CT and image-based modelling is a powerful tool to understand the consequences of the soil structural heterogeneity on soil functions. Indirect modelling methods allow consideration of this structural heterogeneity in an implicit manner. Direct approaches explicitly describe structural heterogeneity. The power of the direct approach is that it allows focus on particular aspects of soil, which often are difficult, or simply impossible, to manipulate experimentally. This strength comes at the cost of requiring higher computing resources which, in practice, limit the volume of soil simulated. These detailed microscale description of soil processes can then be extrapolated to the macroscale using mathematical homogenization.

   Despite providing new insights on soil functioning, the robustness of image-based modelling frameworks relies on the quality of the X-ray CT data, as well as the mathematical and computational tools available. Caution must be made because computation tools may introduce their own errors into the problem being tackled, which can depend on the particular process or components being considered. Another critique often made regarding spatially explicit image-based models, mainly those focused on the soil microscale, is the unfeasibility of 'validating' the model outputs. This is due to the considerable heterogeneity found in soils and to our lack of knowledge of the soil functioning at this scale, which often requires using inverse modelling techniques and educated guesses. In simpler cases of validating image-based models simulating saturated water flow, some discrepancies between the predicted saturated hydraulic conductivity calculated in the X-ray CT images and experimental measures have been reported (Elliot et al., 2010; Dal Ferro et al., 2015; Koestel et al., 2018). This relatively poor performance has been suggested to be related to an inadequate imaging resolution that hinders the visualization of smaller pores in the X-ray CT images that still contribute to the water flow (Dal Ferro et al., 2015; Koestel et al., 2018). The first point to make here is that, in this context, models are first a tool to test and develop alternative hypotheses that can be subsequently tested experimentally. The second point is that when the purpose of modelling is prediction, not being able to obtain a specific experimental measure does not necessarily mean that the model cannot be validated. Confidence in model outputs can be obtained using multiple experimental data or knowledge data measured at different scales and/or for related scenarios (e.g., Grimm et al., 2005). Being able to reproduce situations and outputs for which the model was not explicitly calibrated or designed for suggests that the mechanisms implemented are robust. A closer exchange and collaboration among experimentalist and modellers would revert in the identification of experimental approaches and measurable (indirect) metrics allowing validating current modelling approaches.

A limitation of image-based modelling is inherent to trade-off between sample size and image resolution. The larger the soil sample, the higher the unresolved porosity that we are missing. For some processes such as water flow, this may not be a big deal but for others, such as the ones related to the diffusion of solutes (Zhang et al., 2016) and the biological activity of bacteria and viruses, it may not be acceptable. Decreasing sample size complicates experimental manipulation and may require increasing the number of repetitions. The unresolved porosity issue could be, in principle, partially tackled using greyscale images instead of segmented X-ray CT (Baveye et al., 2017). Reviewing the current work, it is self-evident that very few studies attempt to use this greyscale information which, in our view, should be increasingly explored in the near future. Further opportunities to tackle the resolution limit can also rely on the combination of methods. The representation of reactive species transport in soils, challenging at the time, offers examples of this method combination. In reactive transport, the bottleneck is often associated with the low resolution of X-ray CT images to estimate pore surface area. Some studies have suggested to use a sorption correction function which accounts for the deviation between the complex pore surface area measured in the X-ray CT images and the simpler one generated in an equivalent pore network (Köhne et al., 2011). Such correction functions allow for incorporating the information on the pore surface area into pore network models. Using this strategy, Köhne et al. (2011) improved the transport prediction of a reactive species through intact soil samples. Overall, further studies are required to systematically combine submicron and nanometre scale roughness of soil pore surfaces for accurate prediction of solute and colloid transport. Nanoscale surface heterogeneities have been shown to both increase and decrease colloid attachment in porous surfaces resulted from different influences of roughness under energy barrier absent or present, respectively (Shen et al., 2011; Rasmuson et al., 2017; Torkzaban & Bradford, 2016). As a matter of example, Lin et al. (2021) used a PNM and showed that nanoscale roughness alters the sticking efficiency and colloid attachment non-monotonically with tendency to increase with roughness.

The chapter has also highlighted that the simultaneous use of multi-modal image-based description of the soil is, with few exceptions, still to be translated into modelling exercises. This is the case for imaged organic carbon but, to a certain extent, also for soil microorganisms, although methods are being developed (Baveye et al., 2018). The most common method to date seems to rely on thin slicing of resin impregnated soil cores combined with a specific (FISH) or unspecific (calcofluor white) staining method to visualize microorganisms. These 2-D maps are then aligned with the 3-D structural X-ray CT data following complex alignment procedures (Hapca et al., 2015; Schlüter et al., 2019).

References

Alfaro Soto, M. A., Chang, H. K., & van Genuchten, M. T. (2017). Fractal-based models for the unsaturated soil hydraulic functions. *Geoderma, 306*, 144–151. https://doi.org/10.1016/j.geoderma.2017.07.019

Bastardie, F., Cannavacciuolo, M., Capowiez, Y., de Dreuzy, J.-R., Bellido, A., & Cluzeau, D. (2002). A new simulation for modeling the topology of earthworm burrow systems and their effects on macropore flow in experimental soils. *Biology and Fertility of Soils, 36*, 161–169. https://doi.org/10.1007/s00374-002-0514-0

Baveye, P. C., Pot, V., & Garnier, P. (2017). Accounting for sub-resolution pores in models of water and solute transport in soils based on computed tomography images: Are we there yet? *Journal of Hydrology, 555*, 253–256. https://doi.org/10.1016/j.jhydrol.2017.10.021

Baveye, P. C., Otten, W., Kravchenko, A., Balseiro-Romero, M., Beckers, É., Chalhoub, M., Darnault, C., Eickhorst, T., Garnier, P., Hapca, S., Kiranyaz, S., Monga, O., Mueller, C. W., Nunan, N., Pot, V., Schlüter, S., Schmidt, H., & Vogel, H.-J. (2018). Emergent properties of microbial activity in heterogeneous soil microenvironments: Different research approaches are slowly converging, yet major challenges remain. *Frontiers in Microbiology, 9*, 1929. https://doi.org/10.3389/fmicb.2018.01929

Beckers, E., Plougonven, E., Roisin, C., Hapca, S., Léonard, A., & Degré, A. (2014). X-ray microtomography: A porosity-based thresholding method to improve soil pore network characterization? *Geoderma, 219–220*, 145–154. https://doi.org/10.1016/j.geoderma.2014.01.004

Berg, C. F., & Held, R. (2016). Fundamental transport property relations in porous media incorporating detailed pore structure description. *Transp Porous Med, 112*, 467–487. https://doi.org/10.1007/s11242-016-0661-7

Berg, S., Ott, H., Klapp, S. A., Schwing, A., Neiteler, R., Brussee, N., Makurat, A., Leu, L., Enzmann, F., Schwarz, J.-O., Kersten, M., Irvine, S., & Stampanoni, M. (2013). Real-time 3-D imaging of Haines jumps in porous media flow. *Proceedings of the National Academy of Sciences, 110*, 3755–3759. https://doi.org/10.1073/pnas.1221373110

Blanchart, E., Marilleau, N., Chotte, J.-L., Drogoul, A., Perrier, E., & Cambier, C. (2009). SWORM: An agent-based model to simulate the effect of earthworms on soil structure. *European Journal of Soil Science, 60*, 13–21. https://doi.org/10.1111/j.1365-2389.2008.01091.x

Blank, R. R., & Fosberg, M. A. (1989). Cultivated and adjacent virgin soils in northcentral South Dakota: I. chemical and physical comparisons. *Soil Science Society of America Journal, 53*, 1484–1490. https://doi.org/10.2136/sssaj1989.03615995005300050031x

Blunt, M. J. (2001). Flow in porous media—Pore-network models and multiphase flow. *Curr Opinion Colloid Interf Sci, 6*, 197–207. https://doi.org/10.1016/S1359-0294(01)00084-X

Blunt, M. J., Bijeljic, B., Dong, H., Gharbi, O., Iglauer, S., Mostaghimi, P., Paluszny, A., & Pentland, C. (2013). Pore-scale imaging and modelling. *Advances in Water Resources, 51*, 197–216. https://doi.org/10.1016/j.advwatres.2012.03.003

Bradford, S. A., & Torkzaban, S. (2008). Colloid transport and retention in unsaturated porous media: A review of Interface-, collector-, and pore-scale processes and models. *Vadose Zone Journal, 7*, 667–681. https://doi.org/10.2136/vzj2007.0092

Bultreys, T., De Boever, W., & Cnudde, V. (2016). Imaging and image-based fluid transport modeling at the pore scale in geological materials: A practical introduction to the current state-of-the-art. *Earth-Science Reviews, 155*, 93–128. https://doi.org/10.1016/j.earscirev.2016.02.001

Caplan, J. S., Giménez, D., Subroy, V., Heck, R. J., Prior, S. A., Runion, G. B., & Torbert, H. A. (2017). Nitrogen-mediated effects of elevated CO2 on intra-aggregate soil pore structure. *Glob Change Biol, 23*, 1585–1597. https://doi.org/10.1111/gcb.13496

Capowiez, Y., Pierret, A., Daniel, O., Monestiez, P., & Kretzschmar, A. (1998). 3-D skeleton reconstructions of natural earthworm burrow systems using CAT scan images of soil cores. *Biology and Fertility of Soils, 27*, 51–59. https://doi.org/10.1007/s003740050399

Capowiez, Y., & Belzunces, L. (2001). Dynamic study of the burrowing behavior of *Apporrectodea nocturna* and *Allolobophora chlorotica*: Interactions between earthworm and spatial avoidance of burrows. *Biology and Fertility of Soils, 33*, 310–316. https://doi.org/10.1007/s003740000327

Carminati, A., Kaestner, A., Lehmann, P., & Flühler, H. (2008). Unsaturated water flow across soil aggregate contacts. *Advances in Water Resources, 31*(2008), 1221–1232. https://doi.org/10.1016/j.advwatres.2008.01.008

Carson, J. K., Gonzalez-Quiñones, V., Murphy, D. V., Hinz, C., Shaw, J. A., & Gleeson, D. B. (2010). Low pore connectivity increases bacterial diversity in soil. *Applied and Environmental Microbiology, 76*, 3936–3942. https://doi.org/10.1128/AEM.03085-09

Cazelles, K., Otten, W., Baveye, P. C., & Falconer, R. E. (2013). Soil fungal dynamics: Parameterisation and sensitivity analysis of modelled physiological processes, soil architecture and carbon distribution. *Ecological Modelling, 248*, 165–173. https://doi.org/10.1016/j.ecolmodel.2012.08.008

Clark, T., Burca, G., Boardman, R., & Blumensath, T. (2019). Correlative X-ray and neutron tomography of root systems using cadmium fiducial markers. *Journal of Microscopy, 277*, 170–178. https://doi.org/10.1111/jmi.12831

Cooper, L. J., Daly, K. R., Hallett, P. D., Naveed, M., Koebernick, N., Bengough, A. G., George, T. S., & Roose, T. (2017). Fluid flow in porous media using image-based modelling to parametrize Richards' equation. *Proc.R.Soc.A, 473*, 20170178. https://doi.org/10.1098/rspa.2017.0178

Cooper, L. J., Daly, K. R., Hallett, P. D., Koebernick, N., George, T. S., & Roose, T. (2018). The effect of root exudates on rhizosphere water dynamics. *Proc. R. Soc. A, 474*, 20180149. https://doi.org/10.1098/rspa.2018.0149

Crawford, J. W., Deacon, L., Grinev, D., Harris, J. A., Ritz, K., Singh, B. K., & Young, I. (2012). Microbial diversity affects self-organization of the soil–microbe system with consequences for function. *J. R. Soc. Interface, 9*, 1302–1310. https://doi.org/10.1098/rsif.2011.0679

Crawford, J. W., Ritz, K., & Young, I. (1993). Quantification of fungal morphology, gaseous transport and microbial dynamics in soil: An integrated framework utilising fractal geometry. *Geoderma, 56*, 157–172. https://doi.org/10.1016/0016-7061(93)90107-V

Dal Ferro, N., Charrier, P., & Morari, F. (2013). Dual-scale X-ray CT assessment of soil structure in a long-term fertilization experiment. *Geoderma, 204*, 84–93. https://doi.org/10.1016/j.geoderma.2013.04.012

Dal Ferro, N., Strozzi, A. G., Duwig, C., Delmas, P., Charrier, P., & Morari, F. (2015). Application of smoothed particle hydrodynamics (SPH) and pore morphologic model to predict saturated water conductivity from X-ray CT imaging in a silty loam Cambisol. *Geoderma, 255–256*, 27–34. https://doi.org/10.1016/j.geoderma.2015.04.019

Daly, K. R., & Roose, T. (2014). Multiscale modelling of hydraulic conductivity in vuggy porous media. *Proc. R. Soc. A, 470*, 20130383. https://doi.org/10.1098/rspa.2013.0383

Daly, K. R., & Roose, T. (2015). Homogenization of two fluid flow in porous media. *Proc. R. Soc. A, 471*, 20140564. https://doi.org/10.1098/rspa.2014.0564

Daly, K. R., Mooney, S. J., Bennett, M. J., Crout, N. M., Roose, T., & Tracy, S. R. (2015). Assessing the influence of the rhizosphere on soil hydraulic properties using X-ray computed tomography and numerical modelling. *Journal of Experimental Botany, 66*, 2305–2314. https://doi.org/10.1093/jxb/eru509

Daly, K. R., Keyes, S. D., Masum, S., & Roose, T. (2016). Image based modeling of nutrient movement in and around the rhizosphere. *Journal of Experimental Botany, 67*, 1059–1070. https://doi.org/10.1093/jxb/erv544

Daly, K. R., Cooper, L. J., Koebernick, N., Evaristo, J., Keyes, S. D., van Veelen, A., & Roose, T. (2017). Modelling water dynamics in the rhizosphere. *Rhizosphere, 4*, 139–151. https://doi.org/10.1016/j.rhisph.2017.10.004

Daly, K. R., Tracy, S. R., Crout, N. M. J., Mairhofer, S., Pridmore, T., Mooney, S. J., & Roose, T. (2018). Quantification of root water uptake in soil using X-ray Computed Tomography and image based modelling. *Plant, Cell and Environment, 41*, 121–133. https://doi.org/10.1111/pce.12983

Deurer, M., Müller, K., Kim, I., Huh, K. Y., Young, I., Jun, G. I., & Clothier, B. E. (2012). Can minor compaction increase soil carbon sequestration? A case study in a soil under a wheel-track in an orchard. *Geoderma, 183-184*, 74–79. https://doi.org/10.1016/j.geoderma.2012.02.013

de Paulo, F. L., Surmas, R., Nelis Tonietto, S., Antunes Pereira da Silva, M., & Pires Peçanha, R. (2020). Modeling reactive flow on carbonates with realistic porosity and permeability fields. *Advances in Water Resources, 139*(2020), 103564. https://doi.org/10.1016/j.advwatres.2020.103564

Diel, J., Vogel, H.-J., & Schlüter, S. (2019). Impact of wetting and drying cycles on soil structure dynamics. *Geoderma, 345*, 63–71. https://doi.org/10.1016/j.geoderma.2019.03.018

Dohnal, M., Jelinkova, V., Snehota, M., Dusek, J., & Brezina, J. (2013). Tree-dimensional numerical analysis of water flow affected by entrapped air: Application of noninvasive imaging techniques. *Vadose Zone Journal, 12*, 1–12. https://doi.org/10.2136/vzj2012.0078

Dullien, F. A. L. (1992). Pore structure. In *Porous media*. Elsevier.

Durner, W. (1994). Hydraulic conductivity estimation for soils with heterogeneous pore structure. *Water Resources Resesearch, 30*, 211–233. https://doi.org/10.1029/93WR02676

Ebrahimi, A., Jamshidi, S., Iglauer, S., & Boozarjomehry, R. B. (2013). Genetic algorithm-based pore network extraction from micro-computed tomography images. *Chemical Engineering Science, 92*, 157–166. https://doi.org/10.1016/j.ces.2013.01.045

Ebrahimi, A., & Or, D. (2014). Microbial dispersal in unsaturated porous media: Characteristics of motile bacterial cell motions in unsaturated angular pore networks. *Water Resources Research, 50*, 7406–7429. https://doi.org/10.1002/2014WR015897

Ebrahimi, A., & Or, D. (2015). Hydration and diffusion processes shape microbial community organization and function in model soil aggregates. *Water Resources Research, 51*, 9804–9827. https://doi.org/10.1002/2015WR017565

Elliot, T. R., Reynolds, W. D., & Heck, R. J. (2010). Use of existing pore models and X-ray computed tomography to predict saturated soil hydraulic conductivity. *Geoderma, 156*, 133–142. https://doi.org/10.1016/j.geoderma.2010.02.010

Elyeznasni, N., Sellami, F., Pot, V., Benoit, P., Vieublé-Gonod, L., Young, I., & Peth, S. (2012). Exploration of soil micromorphology to identify coarse-sized OM assemblages in X-ray CT images of undisturbed cultivated soil cores. *Geoderma, 179-180*(38), 45. https://doi.org/10.1016/j.geoderma.2012.02.023

Falconer, R. E., Bown, J. K., White, N. A., & Crawford, J. W. (2005). Biomass recycling and the origin of phenotype in fungal mycelia. *Proceedings of the Royal Society B, 272*, 1727–1734. https://doi.org/10.1098/rspb.2005.3150

Falconer, R. E., Brown, J. L., White, N. A., & Crawford, J. W. (2007). Biomass recycling: A key to efficient foraging by fungal colonies. *Oikos, 116*, 1558–1568. https://doi.org/10.1111/j.2007.0030-1299.15885.x

Falconer, R., Houston, A. N., Otten, W., & Baveye, P. C. (2012). Emergent behavior of soil fungal dynamics: Influence of soil architecture and water distribution. *Soil Science, 177*, 111–119. https://doi.org/10.1097/SS.0b013e318241133a

Falconer, R. E., Battaia, G., Schmidt, S., Baveye, P., Chenu, C., & Otten, W. (2015). Microscale heterogeneity explains experimental variability and non-linearity in soil organic matter mineralisation. *PLoS One, 10*, e0123774. https://doi.org/10.1371/journal.pone.0123774

Gackiewicz, B., Lamorski, K., & Sławiński, C. (2019). Saturated water conductivity estimation based on X-ray CT images–evaluation of the impact of thresholding errors. *International Agrophysics, 33*, 49–60. https://doi.org/10.31545/intagr/104376

Genty, A., & Pot, V. (2013). Numerical simulation of 3-D liquid-gas distribution in porous media by a two-phase TRT lattice Boltzmann method. *Transport in Porous Media, 96*, 271–294. https://doi.org/10.1007/s11242-012-0087-9

Genty, A., & Pot, V. (2014). Numerical calculation of effective diffusion in unsaturated porous media by the TRT lattice Boltzmann method. *Transp Porous Med, 105*, 391–410. https://doi.org/10.1007/s11242-014-0374-8

Gerke, K. M., Vasilyev, R. V., Khirevich, S., Collins, D., Karsanina, M. V., Sizonenko, T. O., Korost, D. V., Lamontagne, S., & Mallants, D. (2018). Finite-difference method stokes solver (FDMSS) for 3-D pore geometries: Software development, validation and case studies. *Computers & Geosciences, 114*, 41–58. https://doi.org/10.1016/j.cageo.2018.01.005

Gerke, K. M., & Karsanina, M. V. (2020). How pore structure non-stationarity compromises flow properties representativity (REV) for soil samples: Pore-scale modelling and stationarity analysis. *European Journal of Soil Science, 72*, 1–19. https://doi.org/10.1111/ejss.13055

Ghanbarian, B., & Hunt, A. G. (2017). Improving unsaturated hydraulic conductivity estimation in soils via percolation theory. *Geoderma, 303*, 9–18. https://doi.org/10.1016/j.geoderma.2017.05.004

Gharedaghloo, B., Price, J. S., Rezanezhad, F., & Quinton, W. L. (2018). Evaluating the hydraulic and transport properties of peat soil using pore network modeling and X-ray micro computed tomography. *Journal of Hydrology, 561*, 494–508. https://doi.org/10.1016/j.jhydrol.2018.04.007

Golparvar, A., Kästner, M., & Thullner, M. (2021). Pore-scale modeling of microbial activity: What we have and what we need. *Vadose Zone Journal, 20*, e20087. https://doi.org/10.1002/vzj2.20087

Gommes, C. J., Bons, A.-J., Blacher, S., Dunsmuir, J. H., & Tsou, A. H. (2009). Practical methods for measuring the tortuosity of porous materials from binary or grey-tone tomographic reconstructions. *AICHE Journal, 55*(8), 2000–2012. https://doi.org/10.1002/aic.11812

Gostick, J., Aghighi, M., Hinebaugh, J., Tranter, T., Hoeh, M. A., Day, H., Spellacy, B., Sharqawy, M. H., Bazylak, A., Burns, A., & Lehnert, W. (2016). OpenPNM: A pore network modeling package. *Computing in Science & Engineering, 18*(4), 60–74. https://doi.org/10.1109/MCSE.2016.49

Gostick, J., Khan, Z. A., Tranter, T. G., Kok, M. D. R., Agnaou, M., Sadeghi, M. A., & Jervis, R. (2019). PoreSpy: A python toolkit for quantitative analysis of porous media images. *Journal of Open Source Software, 4*(37), 1296. https://doi.org/10.21105/joss.01296

Grimm, V., Revilla, E., Berger, U., Jeltsch, F., Wolf, M., Mooij, W. M., Railsback, S. F., Thulke, H.-H., Weiner, J., Wiegand, T., & De Angelis, D. L. (2005). Pattern-oriented modeling of agent-based complex systems: Lessons from ecology. *Science, 310*, 987–991. https://doi.org/10.1126/science.1116681

Hamamoto, S., Moldrup, P., Kawamoto, K., Sakaki, T., Nishimura, T., & Komatsu, T. (2016). Pore network structure linked by X-ray CT to particle characteristics and transport parameters. *Soils and Foundations, 56*(4), 676–690. https://doi.org/10.1016/j.sandf.2016.07.008

Hapca, S. M., Baveye, P. C., Wilson, C., Lark, R. M., & Otten, W. (2015). Three-dimensional mapping of soil chemical characteristics at micrometric scale by combining 2-D SEM-EDX data and 3-D X-Ray CT images. *PLoS One, 10*(9), e0137205. https://doi.org/10.1371/journal.pone.0137205

Hazlett, R. D. (1995). Simulation of capillary-dominated displacements in microtomographic images of reservoir rocks. *Transport in Porous Media, 20*, 21–35. https://doi.org/10.1007/BF00616924

Helliwell, J. R., Sturrock, C. J., Greyling, K. M., Tracy, S. R., Flavel, R. J., Young, I. M., Whalley, W. R., & Mooney, S. J. (2013). Applications of X-ray computed tomography for examining biophysical interactions and structural development in soil systems: A review. *European Journal of Soil Science, 64*, 279–297. https://doi.org/10.1111/ejss.12028

Hilpert, M., & Miller, C. T. (2001). Pore-morphology-based simulation of drainage in totally wetting porous media. *Advances in Water Resources, 24*(3–4), 243–255. https://doi.org/10.1016/S0309-1708(00)00056-7

Hoogland, F., Lehmann, P., Mokso, R., & Or, D. (2016). Drainage mechanisms in porous media: From piston-like invasion to formation of corner flow networks. *Water Resources Research, 52*, 8413–8436. https://doi.org/10.1002/2016WR019299

Hu, W., Liu, G., & Zhang, X. (2018). A pore-scale model for simulating water flow in unsaturated soil. *Microfluidics and Nanofluidics, 22*, 71. https://doi.org/10.1007/s10404-018-2090-0

Hu, X., Li, X.-Y., Li, Z.-C., Gao, Z., Wu, X.-C., Wang, P., Lyu, Y.-L., & Liu, L.-Y. (2020). Linking 3-D soil macropores and root architecture to near saturated hydraulic conductivity of typical meadow soil types in the Qinghai Lake watershed, northeastern Qinghai-Tibet plateau. *Catena, 185*, 104287. https://doi.org/10.1016/j.catena.2019.104287

Hyväluoma, J., Thapaliya, M., Alaraudanjoki, J., Sirén, T., Mattila, K., Timonen, J., & Turtola, E. (2012). Using microtomography, image analysis and flow simulations to characterize soil surface seals. *Computational Geosciences, 48*, 93–101. https://doi.org/10.1016/j.cageo.2012.05.009

Iassonov, P., Gebrenegus, T., & Tuller, M. (2009). Segmentation of X-ray computed tomography images of porous materials: A crucial step for characterization and quantitative analysis of pore structures. *Water Resources Research, 45*, W09415. https://doi.org/10.1029/2009WR008087

Joekar Niasar, V., Hassanizadeh, S. M., Pyrak-Nolte, L. J., & Berentsen, C. (2009). Simulating drainage and imbibition experiments in a high-porosity micromodel using an unstructured pore network model. *Water Resources Research, 45*, W02430. https://doi.org/10.1029/2007WR006641

Joschko, M., Müller, P. C., Kotzke, K., Döhring, W., & Larink, O. (1993). Earthworm burrow system development assessed by means of X-ray computed tomography. *Geoderma, 56*(1–4), 209–221. https://doi.org/10.1016/0016-7061(93)90111-W

Juyal, A., Otten, W., Baveye, P. C., & Eickhorst, T. (2020). Influence of soil structure on the spread of Pseudomonas fluorescens in soil at microscale. *European Journal of Soil Science, 72*, 141–153. https://doi.org/10.1111/ejss.12975

Katuwal, S., Norgaard, T., Moldrup, P., Lamandé, M., Wildenschild, D., & de Jonge, L. W. (2015). Linking air and water transport in intact soils to macropore characteristics inferred from X-ray computed tomography. *Geoderma, 237–238*, 9–20. https://doi.org/10.1016/j.geoderma.2014.08.006

Kasteel, R., Vogel, H.-J., & Roth, K. (2000). From local hydraulic properties to effective transport in soil. *European Journal of Soil Science, 51*, 81–91. https://doi.org/10.1046/j.1365-2389.2000.00282.x

Katz, A. J., & Thompson, A. H. (1986). Quantitative prediction of permeability in porous rock. *Physical Review B, 34*(11), 8179–8181. https://doi.org/10.1103/PhysRevB.34.8179

Kemgue, A. T., Monga, O., Moto, S., Pot, V., Garnier, P., Baveye, P. C., & Bouras, A. (2019). From spheres to ellipsoids: Speeding up considerably the morphological modeling of pore space and water retention in soils. *Computers and Geosciences, 123*, 20–37. https://doi.org/10.1016/j.cageo.2018.11.006

Keyes, S. D., Daly, K. R., Gostling, N. J., Jones, D. L., Talboys, P., Pinzer, B. R., Boardman, R., Sinclair, I., Marchant, A., & Roose, T. (2013). High-resolution synchrotron imaging of wheat root hairs growing in soil and image based modelling of phosphate uptake. *New Phytologist, 198*, 1023–1029. https://doi.org/10.1111/nph.12294

Khan, F., Enzmann, F., Kersten, M., Wiegmann, A., & Steiner, K. (2012). 3-D simulation of the permeability tensor in a soil aggregate on basis of nanotomography imaging and LBE solver. *Journal of Soils and Sediments, 12*, 86–96. https://doi.org/10.1007/s11368-011-0435-3

Kirk, G. J. D., Boghi, A., Affholder, M.-C., Keyes, S. D., Heppell, J., & Roose, T. (2019). Soil carbon dioxide venting through rice roots. *Plant, Cell & Environment, 42*, 3197–3207. https://doi.org/10.1111/pce.13638

Koebernick, N., Daly, K. R., Keyes, S. D., George, T. S., Brown, L. K., Raffan, A., Cooper, L. J., Naveed, M., Bengough, A. G., Sinclair, I., Hallett, P. D., & Roose, T. (2017). High-resolution synchrotron imaging shows that root hairs influence rhizosphere soil structure formation. *The New Phytologist, 216*, 124–135. https://doi.org/10.1111/nph.14705

Koebernick, N., Daly, K. R., Keyes, S. D., Bengough, A. G., Brown, L. K., Cooper, L., George, T. S., Hallett, P. D., Naveed, M., Raffan, A., & Roose, T. (2019). Imaging microstructure of the barley rhizosphere: Particle packing and root hair influences. *New Phytologist, 221*(4), 1878–1889. https://doi.org/10.1111/nph.15516

Koestel, J., Dathe, A., Skaggs, T. H., Klakegg, O., Ahmad, M. A., Babko, M., Giménez, D., Farkas, C., Nemes, A., & Jarvis, N. (2018). Estimating the permeability of naturally structured soil from percolation theory and pore space characteristics imaged by X-Ray. *Water Resources Research, 54*, 9255–9263. https://doi.org/10.1029/2018WR023609

Köhne, M., Schlüter, S., & Vogel, H.-J. (2011). Predicting solute transport in structured soil using pore network models. *Vadose Zone Journal, 10*, 1082–1096. https://doi.org/10.2136/vzj2010.0158

König, S., Vogel, H.-J., Harms, H., & Worrich, A. (2020). Physical, chemical and biological effects on soil bacterial dynamics in microscale models. *Frontiers in Ecology and Evolution, 8*, 53. https://doi.org/10.3389/fevo.2020.00053

Koponen, A., Kataja, M., & Timonen, T. (1996). Tortuous flow in porous media. *Physical Review E, 54*, 406–410. https://doi.org/10.1103/PhysRevE.54.406

Kravchenko, A., Falconer, R. E., Grinev, D., & Otten, W. (2011). Fungal colonization in soils with different management histories: Modeling growth in three-dimensional pore volumes. *Ecological Applications, 21*, 1202–1210. https://doi.org/10.2307/23022990

Kravchenko, A., Guber, A., Gunina, A., Dippold, M., & Kuzyakov, Y. (2020). Pore-scale view of microbial turnover: Combining 14C imaging, µCT and zymography after adding soluble carbon to soil pores of specific sizes. *European Journal of Soil Science, 72*, 593–607. https://doi.org/10.1111/ejss.13001

Larsbo, M., Koestel, J., & Jarvis, N. (2014). Relations between macropore network characteristics and the degree of preferential solute transport. *Hydrology and Earth System Sciences, 18*, 5255–5269. https://doi.org/10.5194/hess-18-5255-2014

Landl, M., Haupenthal, A., Leitner, D., Kroener, E., Vetterlein, D., Bol, R., Vereecken, H., Vanderborght, J., & Schnepf, A. (2021). Simulating rhizodeposition patterns around growing and exuding root systems. *bioRxiv, 2021.02.25.432851*. https://doi.org/10.1101/2021.02.25.432851

Landl, M., Schnepf, A., Uteau, D., Peth, S., Athmann, M., Kautz, T., Perkons, U., Vereecken, H., & Vanderborght, J. (2019). Modeling the impact of biopores on root growth and root water uptake. *Vadose Zone Journal, 18*(1–20), 180196. https://doi.org/10.2136/vzj2018.11.0196

Latt, J., Malaspinas, O., Kontaxakis, D., Parmigiani, A., Lagrava, D., Brogi, F., Ben Belgacem, M., Thorimbert, Y., Leclaire, S., Li, S., Marson, F., Lemus, J., Kotsalos, C., Conradin, R., Coreixas, C., Petkantchin, R., Raynaud, F., Beny, J., & Chopard, B. (2021). Palabos: Parallel Lattice Boltzmann Solver. *Computers & Mathematics with Applications, 81*, 334–350. https://doi.org/10.1016/j.camwa.2020.03.022

Legland, D., Arganda-Carreras, I., & Andrey, P. (2016). MorphoLibJ: Integrated library and plugins for mathematical morphology with ImageJ. *Bioinformatics, 32*, 3532–3534. https://doi.org/10.1093/bioinformatics/btw413

Lehmann, P., Wyss, P., Flisch, A., Lehmann, E., Vontobel, P., Krafczyk, M., Kaestner, A., Beckmann, F., Gygi, A., & Flühler, H. (2006). Tomographical imaging and mathematical description of porous media used for the prediction of fluid distribution. *Vadose Zone Journal, 5*, 80–97. https://doi.org/10.2136/vzj2004.0177

Li, T. C., Shao, M. A., & Jia, Y. H. (2016). Application of X-ray tomography to quantify macropore characteristics of loess soil under two perennial plants. *European Journal of Soil Science, 67*, 266–275. https://doi.org/10.1111/ejss.12330

Li, Z.-S., & Tang, L.-S. (2019). Using synchrotron-based X-Ray microcomputed tomography to characterize water distribution in compacted soils. *Advances in Materials Science and Engineering, 2019*, 7147283.

Lin, D., Hu, L., Bradford, S. A., Zhang, X., & Lo, I. M. C. (2021). Simulation of colloid transport and retention using a pore-network model with roughness and chemical heterogeneity on pore surfaces. *Water Resources Research, 57*, e2020WR028571. https://doi.org/10.1029/2020WR028571

Lin, W., Li, X., Yang, Z., Xiong, S., Luo, Y., & Zhao, X. (2020). Modeling of 3-D rock porous media by combining X-Ray CT and Markov chain Monte Carlo. *ASME Journal Energy Resource Technolology, 142*(1), 013001. https://doi.org/10.1115/1.4045461

Lissy, A.-S., Sammartino, S., & Ruy, S. (2020). Can structure data obtained from CT images substitute for parameters of a preferential flow model? *Geoderma, 380*, 114643. https://doi.org/10.1016/j.geoderma.2020.114643

Liu, L., Dai, S., Ning, F., Cai, J., Liu, C., & Wu, N. (2019). Fractal characteristics of unsaturated sands–implications to relative permeability in hydrate-bearing sediments. *Journal of Natural Gas Science and Engineering, 66*, 11–17. https://doi.org/10.1016/j.jngse.2019.03.019

Long, T., & Or, D. (2005). Aquatic habitats and diffusion constraints affecting microbial coexistence in unsaturated porous media. *Water Resources Research, 41*, W08408. https://doi.org/10.1029/2004WR003796

Lobet, G., Pagès, L., & Draye, X. (2011). A novel image analysis toolbox enabling quantitative analysis of root system architecture. *Plant Physiology, 157*, 29–39. https://doi.org/10.1104/pp.111.179895

Lobet, G., Pound, M. P., Diener, J., Pradal, C., Draye, X., Godin, C., Javaux, M., Leitner, D., Meunier, F., Nacry, P., Pridmore, T. P., & Schnepf, A. (2015). Root system markup language: Toward a unified root architecture description language. *Plant Physiology, 167*, 617–627. https://doi.org/10.1104/pp.114.253625

Luo, L., & Lin, H. (2009). Lacunarity and fractal analyses of soil macropores and preferential transport using micro-X-Ray computed tomography. *Vadose Zone Journal, 8*, 233–241. https://doi.org/10.2136/vzj2008.0010

McKay Fletcher, D. M., Keyes, S. D., Daly, K. R., van Veelen, A., & Roose, T. (2019). A multi image-based approach for modelling plant-fertiliser interaction. *Rhizosphere, 10*, 100152. https://doi.org/10.1016/j.rhisph.2019.100152

McKay Fletcher, D. M., Ruiz, S., Dias, T., Petroselli, C., & Roose, T. (2020). Linking root structure to functionality: The impact of root system architecture on citrate-enhanced phosphate uptake. *The New Phytologist, 227*, 376–391. https://doi.org/10.1111/nph.16554

Mairhofer, S., Johnson, J., Sturrock, C. J., et al. (2016). Visual tracking for the recovery of multiple interacting plant root systems from X-ray μCT images. *Machine Vision and Applications, 27*, 721–734. https://doi.org/10.1007/s00138-015-0733-7

Maenhout, P., De Neve, S., Wragg, J., et al. (2021). Chemical staining of particulate organic matter for improved contrast in soil X-ray CT images. *Scientific Reports, 11*, 370. https://doi.org/10.1038/s41598-020-79681-5

Menon, M., Yuan, Q., Jia, X., Dougill, A. J., Hoon, S. R., Thomas, A. D., & Williams, R. A. (2011). Assessment of physical and hydrological properties of biological soil crusts using X-ray microtomography and modeling. *Journal of Hydrology, 397*, 47–54. https://doi.org/10.1016/j.jhydrol.2010.11.021

Menon, M., Jia, X., Lair, G. J., Faraj, P. H., & Blaud, A. (2015). Analysing the impact of compaction of soil aggregates using X-ray microtomography and water flow simulations. *Soil and Tillage Research, 150*, 147–157. https://doi.org/10.1016/j.still.2015.02.004

Monga, O., Bousso, M., Garnier, P., & Pot, V. (2008). 3-D geometric structures and biological activity: Application to microbial soil organic matter decomposition in pore space. *Ecological Modelling, 216*, 291–302. https://doi.org/10.1016/j.ecolmodel.2008.04.015

Monga, O., Ngom, N. F., & Delerue, J. F. (2007). Representing geometric structures in 3-D tomography soil images: Application to pore space modelling. *Computers and Geosciences, 33*, 1140–1161. https://doi.org/10.1016/j.cageo.2006.11.015

Monga, O., Garnier, P., Pot, V., Coucheney, E., Nunan, N., Otten, W., & Chenu, C. (2014). Simulating microbial degradation of organic matter in a simple porous system using the 3-D diffusion-based model MOSAIC. *Biogeosciences, 11*, 2201–2209. https://doi.org/10.5194/bg-11-2201-2014

Mooney, S. (2002). Three-dimensional visualization and quantification of soil macroporosity and water flow patterns using computed tomography. *Soil Use and Management, 18*, 142–151. https://doi.org/10.1111/j.1475-2743.2002.tb00232.x

Moradi, A. B., Carminati, A., Vetterlein, D., Vontobel, P., Lehmann, E., Weller, U., Hopmans, J. W., Vogel, H. J., & Oswald, S. E. (2011). Three-dimensional visualization and quantification of water content in the rhizosphere. *The New Phytologist, 192*(3), 653–663. https://doi.org/10.1111/j.1469-8137.2011.03826.x

Ngom, N. F., Garnier, P., Monga, O., & Peth, S. (2011). Extraction of three-dimensional soil pore space from microtomography images using a geometrical approach. *Geoderma, 163*, 127–134. https://doi.org/10.1016/j.geoderma.2011.04.013

Ngom, N. F., Monga, O., Mohamed, M. M. O., & Garnier, P. (2012). 3-D shape extraction segmentation and representation of soil microstructures using generalized cylinders. *Computers & Geosciences, 39*, 50–63. https://doi.org/10.1016/j.cageo.2011.06.010

Nishiyama, N., & Yokoyama, T. (2017). Permeability of porous media: Role of the critical pore size. *Journal of Geophysical Research–Solid Earth, 122*, 6955–6971. https://doi.org/10.1002/2016JB013793

Pagenkemper, S. K., Athmann, M., Uteau, D., Kautz, T., Peth, S., & Horn, R. (2015). The effect of earthworm activity on soil bioporosity–investigated with X-ray computed tomography and endoscopy. *Soil and Tillage Research, 146*(Part A), 79–88. https://doi.org/10.1016/j.still.2014.05.007

Pajor, R., Falconer, R., Hapca, S., & Otten, W. (2010). Modelling and quantifying the effect of heterogeneity in soil physical conditions on fungal growth. *Biogeosciences, 7*, 3477–3501. https://doi.org/10.5194/bg-7-3731-2010

Papadopoulos, A., Bird, N. R. A., Whitmore, A. P., & Mooney, S. J. (2009). Investigating the effects of organic and conventional management on soil aggregate stability using X-ray computed tomography. *European Journal of Soil Science, 60*, 360–368. https://doi.org/10.1111/j.1365-2389.2009.01126.x

Perez-Reche, F. J., Taraskin, S. N., Otten, W., Viana, M. P., Costa, L. F., & Gilligan, C. A. (2012). Prominent effect of soil network heterogeneity on microbial invasion. *Physical Review Letters, 109*, 098102. https://doi.org/10.1103/PhysRevLett.109.098102

Peszynska, M., Trykozko, A., Iltis, G., Schlüter, S., & Wildenschild, W. (2016). Biofilm growth in porous media: Experiments, computational modeling at the porescale, and upscaling. *Advances in Water Resources, 95*, 288–301. https://doi.org/10.1016/j.advwatres.205.07.008

Peth, S., Chenu, C., Leblond, N., Mordhorst, A., Garnier, P., Nunan, N., Pot, V., Ogurreck, M., & Beckmann, F. (2014). Localization of soil organic matter in soil aggregates using synchrotron-based X-ray microtomography. *Soil Biology & Biochemistry, 78*, 189e194. https://doi.org/10.1016/j.soilbio.2014.07.024

Piccoli, I., Dal Ferro, N., Delmas, P. J., Squartini, A., & Morari, F. (2019a). Contrast-enhanced repacked soil cores as a proxy for soil organic matter spatial arrangement. *Soil Research, 57*, 535–545. https://doi.org/10.1071/SR18191

Piccoli, I., Schjønning, P., Lamandé, M., Zanini, F., & Morari, F. (2019b). Coupling gas transport measurements and X-ray tomography scans for multiscale analysis in silty soils. *Geoderma, 338*, 576–584. https://doi.org/10.1016/j.geoderma.2018.09.029

Porre, R. J., van Groenigen, J. W., De Deyn, G. B., de Goede, R. G. M., & Lubbers, I. M. (2016). Exploring the relationship between soil mesofauna, soil structure and N2O emissions. *Soil Biology and Biochemistry, 96*, 55–64. https://doi.org/10.1016/j.soilbio.2016.01.018

Portell, X., Pot, V., Garnier, P., Otten, W., & Baveye, P. C. (2018). Microscale heterogeneity of the spatial distribution of organic matter can promote bacterial biodiversity in soils: Insights from computer simulations. *Frontiers in Microbiology, 9*, 1583. https://doi.org/10.3389/fmicb.2018.01583

Pot, V., Hammou, H., Elyeznasni, N., Ginburg, I. (2010). *Role of soil heterogeneities onto pesticide fate: A pore-scale study with lattice Boltzmann*. 1st International conference and exploratory workshop on soil architecture and physico-chemical functions, CESAR, Tjele, Danemark (2010-11-30–2010-12-02) pp. 307–310.

Pot V, Peth S, Garnier P, Genty A, Monga O, Vieublé-Gonod L, Pinheiro M, Ogurreck M, Beckmann F (2011, June–July 26). *Visualisation and modelling of water-air interface in soil porosity: impact on microbial degradation*. Poster presented at the Soil Interfaces in a Changing World 6th ISMOM 2011 Conference.

Pot, V., Peth, S., Monga, O., Vogel, L. E., Genty, A., Garnier, P., Vieublé-Gonod, L., Ogurreck, M., Beckmann, F., & Baveye, P. C. (2015). Three-dimensional distribution of water and air in soil pores: Comparison of two-phase two-relaxation-times lattice-Boltzmann and morphological model outputs with synchrotron X-ray computed tomography data. *Advances in Water Resources, 84*, 87–102. https://doi.org/10.1016/j.advwatres.2015.08.006

Pot, V., Zhong, X., & Baveye, P. C. (2020). Effect of resolution, reconstruction settings, and segmentation methods on the numerical calculation of saturated soil hydraulic conductivity from 3-D computed tomography images. *Geoderma, 362*, 114089. https://doi.org/10.1016/j.geoderma.2019.114089

Quigley, M. Y., Rivers, M. L., & Kravchenko, A. N. (2018). Patterns and sources of spatial heterogeneity in soil matrix from contrasting Long term management practices. *Frontiers in Environmental Science, 6*, 28. https://doi.org/10.3389/fenvs.2018.00028

Rabbi, S. M. F., Tighe, M. K., Flavel, R. J., Kaiser, B. N., Guppy, C. N., Zhang, X., & Young, I. M. (2018). Plant roots redesign the rhizosphere to alter the three-dimensional physical architecture and water dynamics. *New Phytologist, 219*, 542–550. https://doi.org/10.1111/nph.15213

Rabot, E., Cousin, I., & Hénault, C. A. (2015). Modeling approach of the relationship between nitrous oxide fluxes from soils and the water-filled pore space. *Biogeochemistry, 122*, 395–408. https://doi.org/10.1007/s10533-014-0048-1

Raoof, A., & Hassanizadeh, S. M. (2012). A new formulation for pore-network modeling of two-phase flow. *Water Resource Research, 48*, W01514. https://doi.org/10.1029/2010WR010180

Rasmuson, A., Pazmino, E., Assemi, S., & Johnson, W. P. (2017). Contribution of Nano- to microscale roughness to heterogeneity: Closing the gap between unfavorable and favorable colloid attachment conditions. *Environmental Science & Technology, 51*, 2151–2160. https://doi.org/10.1021/acs.est.6b05911

Ray, N., Rupp, A., & Prechtel, A. (2017). Discrete-continuum multiscale model for transport, biomass development and solid restructuring in porous media. *Advances in Water Resources, 107*, 393–404. https://doi.org/10.1016/j.advwatres.2017.04.001

Resat, H., Bailey, V., McCue, L. A., & Konpka, A. (2012). Modeling microbial dynamics in heterogeneous environments: Growth on soil carbon sources. *Microbial Ecology, 63*, 883–897. https://doi.org/10.1007/s00248-011-9965-x

Rezanezhad, F., Quinton, W. L., Price, J. S., Elrick, D., Elliot, T. R., & Heck, R. J. (2009). Examining the effect of pore size distribution and shape on flow through unsaturated peat using computed tomography. *Hydrology and Earth System Sciences, 13*, 1993–2002. https://doi.org/10.5194/hess-13-1993-2009

Rezanezhad, F., Quinton, W. L., Price, J. S., Elliot, T. R., Elrick, D., & Shook, K. R. (2010). Influence of pore size and geometry on peat unsaturated hydraulic conductivity computed from 3-D computed tomography image analysis. *Hydrological Processes, 24*, 2983–2994. https://doi.org/10.1002/hyp.7709

Roose, T., & Fowler, A. C. (2004). A model for water uptake by plant roots. *Journal of Theoretical Biology, 228*, 155–171. https://doi.org/10.1016/j.jtbi.2003.12.012

Roose, T., Keyes, S., Daly, K., Carminati, A., Otten, W., Vetterlein, D., & Peth, S. (2016). Challenges in imaging and predictive modeling of rhizosphere processes. *Plant and Soil, 407*, 9–38. https://doi.org/10.1007/s11104-016-2872-7

Roque, W. L., & Costa, R. R. A. (2020). A plugin for computing the pore/grain network tortuosity of a porous medium from 2-D/3-D MicroCT image. *Applied Computing and Geosciences., 5*, 100019. https://doi.org/10.1016/j.acags.2020.100019

Ruiz, S. A., McKay Fletcher, D. M., Boghi, A., Williams, K. A., Duncan, S. J., Scotson, C. P., Petroselli, C., Dias, T. G. S., Chadwick, D. R., Jones, D. L., & Roose, T. (2020a). Image-based quantification of soil microbial dead zones induced by nitrogen fertilization. *Science Total Environment, 727*, 138197. https://doi.org/10.1016/j.scitotenv.2020.138197

Ruiz, S. A., Mckay Fletcher, D., Williams, K., Roose, T. (2020b). Review of plant-soil modelling: Root growth, nutrient and water transport/uptake, and mechanics. *Annual Plant Reviews*.

San José Martínez, F., Martín, M. A., Caniego, F. J., Tuller, M., Guber, A., Pachepsky, Y., & García-Gutiérrez, C. (2010). Multifractal analysis of discretized X-ray CT images for the characterization of soil macropore structures. *Geoderma, 156*, 32–42. https://doi.org/10.1016/j.geoderma.2010.01.004

Saiers, J. E., & Lenhart, J. J. (2003). Colloid mobilization and transport within unsaturated porous media under transient-flow conditions. *Water Resources Research, 39*, 1019. https://doi.org/10.1029/2002WR001370

Schaap, M. G., Porter, M. L., Christensen, B. S. B., & Wildenschild, D. (2007). Comparison of pressure-saturation characteristics derived from computed tomography and lattice Boltzmann simulations. *Water Resources Research, 43:W12S06*. https://doi.org/10.1029/2006WR005730

Schlüter, S., Sheppard, A., Brown, K., & Wildenschild, D. (2014). Image processing of multiphase images obtained via X-ray microtomography: A review. *Water Resources Research, 50*, 3615–3639. https://doi.org/10.1002/2014WR015256

Schlüter, S., Eickhorst, T., & Mueller, C. W. (2019). Correlative imaging reveals holistic view of soil microenvironments. *Environmental Science & Technology, 53*, 829–837. https://doi.org/10.1021/acs.est.8b05245

Schnepf, A., Black, C. K., Couvreur, V., Delory, B. M., Doussan, C., Koch, A., Koch, T., Javaux, M., Landl, M., Leitner, D., Lobet, G., Mai, T. H., Meunier, F., Petrich, L., Postma, J. A., Priesack, E., Schmidt, V., Vanderborght, J., Vereecken, H., & Weber, M. (2020). Call for participation: Collaborative benchmarking of functional-structural root architecture models. The case of root water uptake. *Frontiers in Plant Science, 11*(316). https://doi.org/10.3389/fpls.2020.00316

Scotson, C. P., Munoz-Hernando, M., Duncan, S. J., Ruiz, S. A., Keyes, S. D., van Veelen, A., Dunlop, I. E., & Roose, T. (2019). Stabilizing gold nanoparticles for use in X-ray computed tomography imaging of soil systems. *Royal Society Open Science, 6190769190769*. https://doi.org/10.1098/rsos.190769

Shen, C., Li, B., Wang, C., Huang, Y., & Jin, Y. (2011). Surface roughness effect on deposition of nano- and micro-sized colloids in saturated columns at different solution ionic strengths. *Vadose Zone Journal, 10*, 1071–1081. https://doi.org/10.2136/vzj2011.0011

Seaton, M. A., Anderson, R. L., Metz, S., & Smith, W. (2013). DL_MESO: Highly scalable mesoscale simulations. *Molecular Simulation, 39*(10), 796–821. https://doi.org/10.1080/08927022.2013.772297

Soto-Gómez, D., Pérez-Rodríguez, P., Vázquez-Juiz, L., López-Periago, E., & Paradelo, M. (2018). Linking pore network characteristics extracted from CT images to the transport of solute and colloid tracers in soils under different tillage managements. *Soil and Tillage Research, 177*, 145–154. https://doi.org/10.1016/j.still.2017.12.007

Spanne, P., Thovert, J. F., Jacquin, C. J., Lindquist, W. B., Jones, K. W., & Adler, P. M. (1994). Synchrotron computed microtomography of porous media: Topology and transports. *Physical Review Letters, 73*, 2001–2004. https://doi.org/10.1103/PhysRevLett.73.2001

Sukop, M. C., Huang, H., Lin, C. L., Deo, M. D., Oh, K., & Miller, J. D. (2008). Distribution of multiphase fluids in porous media: Comparison between lattice Boltzmann modeling and

micro-x-ray tomography. *Physical Review E, 77*, 026710. https://doi.org/10.1103/PhysRevE.77.026710

Tecon, R., Ebrahimi, A., Kleyer, H., Levi, S. E., & Or, D. (2018). Cell-to-cell bacterial interactions promoted by drier conditions on soil surfaces. *PNAS, 115*, 9791–9796. https://doi.org/10.1073/pnas.1808274115

Torkzaban, S., & Bradford, S. A. (2016). Critical role of surface roughness on colloid retention and release in porous media. *Water Research, 88*, 274–284. https://doi.org/10.1016/j.watres.2015.10.022

Tötzke, C., Kardjilov, N., Hilger, A., Rudolph-Mohr, N., Manke, I., & Oswald, S. E. (2021). Three-dimensional in vivo analysis of water uptake and translocation in maize roots by fast neutron tomography. *Scientific Reports, 11*, 10578. https://doi.org/10.1038/s41598-021-90062-4

Tran, A. P., Yan, S., & Fang, Q. (2020). Improving model-based functional near-infrared spectroscopy analysis using mesh-based anatomical and light-transport models. *Neurophotonics, 7*, 015008. https://doi.org/10.1117/1.NPh.7.1.015008

Tuller, M., Or, D., & Dudley, L. M. (1999). Adsorption and capillary condensation in porous media: Liquid retention and interfacial configurations in angular pores. *Water Resources Research, 35*(7), 1949–1964. https://doi.org/10.1029/1999WR900098

Tuller, M., & Or, D. (2001). Hydraulic conductivity of variably saturated porous media: Film and corner flow in angular pore space. *Water Resources Research, 37*(5), 1257–1276. https://doi.org/10.1029/2000WR900328

Tyler, S. W., & Wheatcraft, S. W. (1990). Fractal processes in soil water retention. *Water Resources Research, 26*(5), 1047–1054. https://doi.org/10.1029/WR026i005p01047

Valvatne, P. H., & Blunt, M. J. (2004). Predictive pore-scale modeling of two-phase flow in mixed wet media. *Water Resources Research, 40*, W07406. https://doi.org/10.1029/2003WR002627

van Genuchten, M. (1980). A closed-form equation for predicting the hydraulic conductivity of unsaturated soils. *Soil Science Society of America Journal, 44*, 892–898. https://doi.org/10.2136/sssaj1980.03615995004400050002x

Van Loo, D., Bouckaert, L., Leroux, O., Pauwels, E., Dierick, M., Van Hoorebeke, L., Cnudde, V., De Neve, S., & Sleutel, S. (2014). Contrast agents for soil investigation with X-ray computed tomography. *Geoderma, 213*, 485–491. https://doi.org/10.1016/j.geoderma.2013.08.036

Vogel, H.-J. (2008). *QuantIm–some useful C/C++ functions for scientific image processing*. Helmholtz Center for Environmental Research.

Vogel, H.-J., & Roth, K. (2001). Quantitative morphology and network representation of soil pore structure. *Advances in Water Resources, 24*, 233–242. https://doi.org/10.1016/S0309-1708(00)00055-5

Vogel, H.-J., Tölke, J., Schulz, V. P., Krafczyk, M., & Roth, K. (2005). Comparison of a Lattice-Boltzmann model, a full-morphology model, and a pore network model for determining capillary pressure–saturation relationships. *Vadose Zone Journal, 4*, 380–388. https://doi.org/10.2136/vzj2004.0114

Vogel, L., Makowski, D., Garnier, P., Vieublé-Gonod, L., Coquet, Y., Raynaud, X., Nunan, N., Chenu, C., Falconer, R., & Pot, V. (2015). Modeling the effect of soil meso- and macropores topology on the biodegradation of a soluble carbon substrate. *Advances in Water Resources, 83*, 123–126. https://doi.org/10.1016/j.advwatres.2015.05.020

Vogel, L., Pot, V., Makowski, D., Garnier, P., & Baveye, P. C. (2018). To what extent do uncertainty and sensitivity analyses help unravel the influence of microscale physical and biological drivers in soil carbon dynamics models? *Ecological Modelling, 383*, 10–22. https://doi.org/10.1016/j.ecolmodel.2018.05.007

Wu, K., Nunan, N., Crawford, J. W., Young, I. M., & Ritz, K. (2004). An efficient Markov chain model for the simulation of heterogeneous soil structure. *Soil Science Society of America Journal, 68*, 346–351. https://doi.org/10.2136/sssaj2004.3460

Xiong, Q., Baychev, T. G., & Jivkov, A. P. (2016). Review of pore network modelling of porous media: Experimental characterisations, network constructions and applications to reactive

transport. *Journal of Contaminant Hydrology, 192*, 101–117. https://doi.org/10.1016/j.jconhyd.2016.07.002

Xu, Y. (2004). Calculation of unsaturated hydraulic conductivity using a fractal model for the pore-size distribution. *Computers and Geotechnics, 31*, 549–557. https://doi.org/10.1016/j.compgeo.2004.07.003

Yu, B., & Liu, W. (2004). Fractal analysis of permeabilities for porous media. *American Institute of Chemical Engineers Journal, 50*, 46–57. https://doi.org/10.1002/aic.10004

Zarebanadkouki, M., Kim, Y., Moradi, A., Vogel, H.-J., Kaestner, A., & Carminati, A. (2012). Quantification and modeling of local root water uptake using neutron radiography and deuterated water. *Vadose Zone Journal, 11*(vzj2011), 0196. https://doi.org/10.2136/vzj2011.0196

Zarebanadkouki, M., Kroener, E., Kaestner, A., & Carminati, A. (2014). Visualization of root water uptake: Quantification of deuterated water transport in roots using neutron radiography and numerical modelling. *Plant Physiology, 166*, 487–499. https://doi.org/10.1104/pp.114.243212

Zhang, X., Crawford, J. W., Flavel, R. J., & Young, I. M. (2016). A multi-scale lattice Boltzmann model for simulating solute transport in 3-D X-ray micro-tomography images of aggregated porous materials. *Journal of Hydrology, 541*, 1020–1029. https://doi.org/10.1016/j.jhydrol.2016.08.013

Zhang, X., Neal, A. L., Crawford, J. W., Bacq-Labreuil, A., Akkari, E., & Rickard, W. (2021a). The effects of long-term fertilizations on soil hydraulic properties vary with scales. *Journal of Hydrology, 593*, 125890. https://doi.org/10.1016/j.jhydrol.2020.125890

Zhang, Y., Yang, Z., Wang, F., & Zhang, X. (2021b). Comparison of soil tortuosity calculated by different methods. *Geoderma, 402*, 115358. https://doi.org/10.1016/j.geoderma.2021.115358

Zheng, H., Kim, K., Kravchenko, A., Rivers, M., & Guber, A. (2020). Testing Os staining approach for visualizing soil organic matter patterns in intact samples via X-ray dual-energy tomography scanning. *Environmental Science & Technology, 54*, 8980–8989. https://doi.org/10.1021/acs.est.0c01028

Zhou, M., Lu, D., Dunsmuir, J., & Thomann, H. (2000). Irreducible water distribution in sandstone rock: Two phase flow simulations in CT-based pore network. *Physics and Chemistry of the Earth, Part A: Solid Earth and Geodesy, 25*(2), 169–174. https://doi.org/10.1016/S1464-1895(00)00027-2

Zhou, H., Yu, X., Chen, C., Zeng, L., Lu, S., & Wu, L. (2018). Evaluating hydraulic properties of biochar-amended soil aggregates by high-performance pore-scale simulations. *Soil Science Society of America Journal, 82*, 1–9. https://doi.org/10.2136/sssaj2017.02.0053

Zhou, H., Yu, X., Chen, C., Lu, S., Wu, L., & Zeng, L. (2019). Pore-scale lattice Boltzmann modeling of solute transport in saturated biochar amended soil aggregates. *Journal of Hydrology, 577*, 123933. https://doi.org/10.1016/j.jhydrol.2019.123933